

Mid-Air Drawing of Curves on 3D Surfaces in Virtual Reality

RAHUL ARORA, University of Toronto, Canada

KARAN SINGH, University of Toronto, Canada

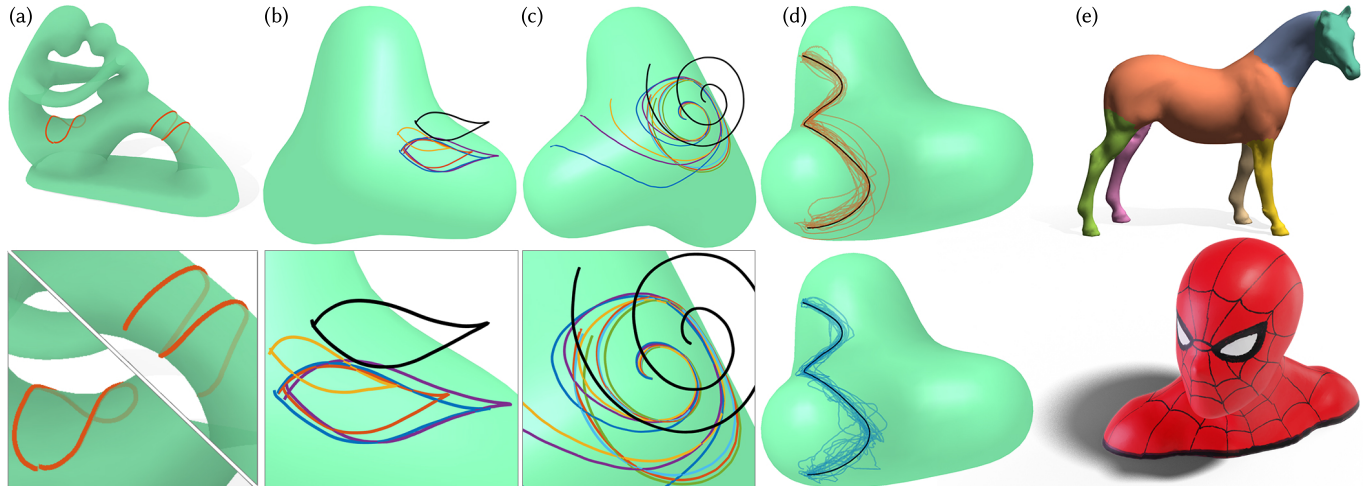


Fig. 1. Drawing curves mid-air that lie precisely on the surface of a virtual 3D object in AR/VR is difficult (a). Projecting mid-air 3D strokes (**black**) onto 3D objects is an under-constrained problem with many seemingly reasonable solutions (b). We analyze this fundamental AR/VR problem of 3D stroke projection, define and characterize multiple novel projection techniques (c), and test the two most promising approaches—*spraycan* shown in **blue** and *mimicry* shown in **red** in (b)–(d)—using a quantitative study with 20 users (d). The user-preferred *mimicry* technique attempts to mimic the 3D mid-air stroke as closely as possible when projecting onto the virtual object. We showcase the importance of drawing curves on 3D surfaces, and the utility of our novel *mimicry* approach, using multiple artistic and functional applications (e) such as interactive shape segmentation (top) and texture painting (bottom).

Complex 3D curves can be created by directly drawing mid-air in immersive environments (Augmented and Virtual Realities). Drawing mid-air strokes precisely on the surface of a 3D virtual object, however, is difficult; necessitating a projection of the mid-air stroke onto the user “intended” surface curve. We present the first detailed investigation of the fundamental problem of 3D stroke projection in VR. An assessment of the design requirements of real-time drawing of curves on 3D objects in VR is followed by the definition and classification of multiple techniques for 3D stroke projection. We analyze the advantages and shortcomings of these approaches both theoretically and via practical pilot testing. We then formally evaluate the two most promising techniques *spraycan* and *mimicry* with 20 users in VR. The study shows a strong qualitative and quantitative user preference for our novel stroke *mimicry* projection algorithm. We further illustrate the effectiveness and utility of stroke mimicry, to draw complex 3D curves on surfaces for various artistic and functional design applications.

CCS Concepts: • **Human-centered computing** → **Virtual reality**; • **Computing methodologies** → **Graphics systems and interfaces**; *Shape modeling*.

Additional Key Words and Phrases: 3D sketching; curve on surface; AR/VR

1 INTRODUCTION

Drawing is a fundamental tool of human visual expression and communication. Digital sketching with pens, styli, mice, and even fingers in 2D is ubiquitous in visually creative computing applications. Drawing or painting **on** 3D virtual objects for example, is critical to interactive 3D modelling, animation, and visualization,

where its uses include: object selection, annotation, and segmentation [Heckel et al. 2013; Jung et al. 2002; Meng et al. 2011]; 3D curve and surface design [Igarashi et al. 1999; Nealen et al. 2007]; strokes for 3D model texturing or painterly rendering [Kalnins et al. 2002] (Figure 1e). In 2D, digitally drawn on-screen strokes are WYSIWYG mapped onto 3D virtual objects, by projecting 2D stroke points through the given view onto the virtual object(s) (Figure 2a).

Sketching in immersive environments (AR/VR) has the mystical aura of a magical wand, allowing users to draw directly in 3D. Mid-air drawing has the potential to significantly disrupt interactive 3D graphics, as evidenced by the increasing popularity of applications such as Tilt Brush [Google 2020] and Quill [Oculus 2020]. A fundamental requirement for numerous interactive 3D applications in AR/VR is the ability to directly draw, or project drawn 3D strokes, precisely on virtual objects. While directly drawing on a physical object is reasonably easy, drawing directly on a virtual 3D object is near impossible without haptic constraints (Figure 3). Furthermore, unlike 2D drawing, where the WYSIWYG view-based projection of 2D strokes onto 3D objects is unambiguously clear, the user-intended mapping of a mid-air 3D stroke onto a 3D object is less obvious. We present the first detailed investigation into plausible user-intended projections of mid-air strokes on to 3D virtual objects.

Interfaces for 2D/3D curve creation in general, use perceptual insights or geometric assumptions like smoothness and planarity, to project, neaten, or otherwise process sketched strokes. Some applications wait for user stroke completion before processing it

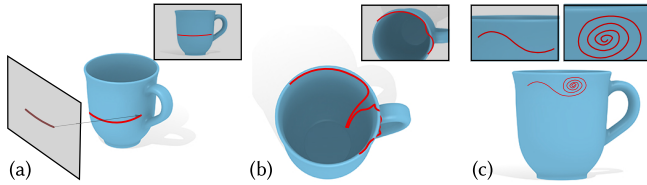


Fig. 2. Stroke projection using a 2D interface is typically WYSIWYG: 2D points along a user stroke (a, inset) are ray-cast through the given view to create corresponding 3D curve points on the surface of 3D scene objects (a). Even small errors or noise in 2D strokes can cause large discontinuities in 3D, especially near ridges and sharp features (b). Complex curves spanning many viewpoints, or with large scale variations in detail, often require the curve to be drawn in segments from multiple user-adjusted viewpoints (c).

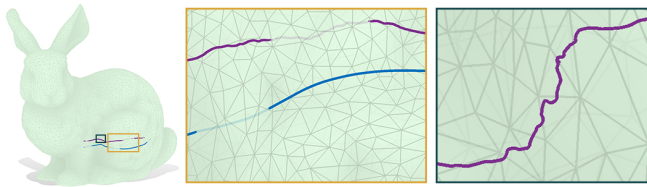


Fig. 3. Mid-air drawing precisely on a 3D virtual object is difficult (faint regions of strokes are behind the surface), regardless of drawing quick smooth strokes (blue), or slow detailed strokes (purple). Deliberately slow drawing is further detrimental to stroke aesthetic (right).

in entirety, for example when fitting splines [Bae et al. 2008]. Our goal is to establish an application agnostic, base-line projection approach for mid-air 3D strokes. We thus assume a stroke is processed while being drawn and inked in real-time, i.e., the output curve corresponding to a partially drawn stroke is fixed/inked in real-time, based on partial stroke input [Thiel et al. 2011].

One might further conjecture that all “reasonable” and mostly continuous projections would produce similar results, as long as users are given interactive visual feedback of the projection. This is indeed true for tasks requiring discrete point-on-surface selection, where users can freely re-position the drawing tool until its interactively visible projection corresponds to user-intent. Real-time curve drawing, however, is very sensitive to the projection technique, where any mismatch between user intention and algorithmic projection, is continuously inked into the projected curve (Figure 1d).

2D Strokes Projected onto 3D Objects. The standard user-intended mapping of a 2D on-screen stroke is a raycast projection through the given monocular viewpoint. Raycasting is WYSIWYG (What You See Is What You Get): the 3D curve visually matches the 2D stroke from said viewpoint (Figure 2a). Ongoing research on mapping 2D strokes to 3D objects assumes this fundamental *view-centric* projection, focusing instead on specific problems such as creating curves around ridge/valley features (where small 2D error can cause large 3D depth error, Figure 2b); or drawing complex curves with large scale variation (where multiple viewpoint changes are needed while drawing, Figure 2c). These problems are mitigated by the direct 3D input and viewing flexibility of AR/VR, assuming the mid-air stroke to 3D object projection matches user intent.

3D Strokes Projected onto 3D Objects. Physical analogies motivate existing approaches to defining a user-intended projection from 3D points in a mid-air stroke to 3D points on a virtual object (Figure 4). Graffiti-style painting with a *spraycan* is arguably the current standard, deployed in commercial immersive paint and sculpt software such as Medium [Adobe 2021] and Gravity Sketch [2020]. A closest-point projection approximates drawing with the tool on the 3D object, without actual physical contact (used by the “guides” tool in Tilt Brush [Google 2020]). Like view-centric 2D stroke projection, these approaches are *context-free*: processing each mid-air point independently. The AR/VR drawing environment comprising six-degree of freedom controller input and unconstrained binocular viewing, is however, significantly richer than 2D sketching. The user-intended projection of a mid-air stroke (§ 3) as a result is complex, influenced by the ever-changing 3D relationship between the view, drawing controller and virtual object. We therefore argue the need for historical context (i.e., the partially drawn stroke and its projection) in determining the projection of a given stroke point. We balance the use of this historical context, with the overarching goal of a general purpose projection that makes little or no assumption on the nature of the user stroke or its projection.

We thus explore *anchored* projection techniques, that minimally use the most recently projected stroke point, as context for projecting the current stroke point (§ 4). We evaluate various anchored projections, both theoretically and practically by pilot testing. Our most promising and novel approach *anchored-smooth-closest-point* (also called *mimicry*), captures the natural tendency of a user stroke to mimic the shape of the desired projected curve. A formal user study in VR (§ 5) shows *mimicry* to perform significantly better than *spraycan* (the current baseline) in producing curves that match user intent (§ 6). While our formal evaluation is limited to VR, the fundamental problem we study could directly translate to AR scenarios as well. This paper thus contributes, to the best of our knowledge, the first principled investigation of real-time inked techniques to project 3D mid-air strokes drawn in VR onto 3D virtual objects, and a novel stroke projection benchmark for VR: *mimicry*.

2 RELATED WORK

Our work is related to research on drawing and sculpting in immersive realities, interfaces for drawing curves on, near, and around surfaces, and sketch-based modelling tools.

2.1 Immersive Sketching and Modelling

Immersive creation has a long history in computer graphics. Immersive 3D sketching was pioneered by the HoloSketch system [Deering 1995], which used a 6-DoF wand as the input device for creating polyline sketches, 3D tubes, and primitives. In a similar vein, various subsequent systems have explored the creation of freeform 3D curves and swept surfaces [Google 2020; Keefe et al. 2001; Schkolne et al. 2001]. While directly turning 3D input to creative output is acceptable for ideation, the inherent imprecision of 3D sketching is quickly apparent when more structured creation is desired.

The perceptual and ergonomic challenges in precise control of 3D input is well-known [Arora et al. 2017; Keefe et al. 2007; Machuca et al. 2018, 2019; Wiese et al. 2010], resulting in various methods

for correcting 3D input. Input 3D curves have been algorithmically regularized to snap onto existing geometry, as with the FreeDrawer [Wesche and Seidel 2001] system, or constrained physically to 2D input with additional techniques for “lifting” these curves into 3D [Arora et al. 2018; Jackson and Keefe 2016; Kwan and Fu 2019; Paczkowski et al. 2011]. Haptic rendering devices [Kamuro et al. 2011; Keefe et al. 2007] and tools utilizing passive physical feedback [Grossman et al. 2002] are an alternate approach to tackling the imprecision of 3D inputs. We are motivated by similar considerations.

Arora et al. [2017] demonstrated the difficulty of creating curves that lie exactly on virtual surfaces in VR, even when the virtual surface is a plane. This observation directly motivates our exploration of techniques for projecting 3D strokes onto surfaces, instead of coercing users to awkwardly draw exactly on a virtual surface.

2.2 Drawing Curves on, near, and around Surfaces

Curve creation and editing on or near the surface of 3D virtual objects is fundamental for a variety of artistic and functional shape modelling tasks. Functionally, curves on 3D surfaces are used to model or annotate structural features [Gal et al. 2009; Stanculescu et al. 2013], define trims and holes [Schmidt and Singh 2010], and to provide handles for shape deformation [Kara and Shimada 2007; Nealen et al. 2007; Singh and Fiume 1998], registration [Gehre et al. 2018] and remeshing [Krishnamurthy and Levoy 1996; Takayama et al. 2013]. Artistically, curves on surfaces are used in painterly rendering [Gooch and Gooch 2001], decal creation [Schmidt et al. 2006], texture painting [Adobe 2020], and even texture synthesis [Fisher et al. 2007]. Curve on surface creation in this body of research typically uses the established view-centric WYSIWYG projection of on-screen sketched 2D strokes. While the sketch view-point in these interfaces is interactively set by the user, there has been some effort in automatic camera control for drawing [Ortega and Vincent 2014], auto-rotation of the sketching view for 3D planar curves [McCrae et al. 2014], and user assistance in selecting the most *sketchable* viewpoints [Bae et al. 2008]. Immersive 3D drawing enables direct, view-point independent 3D curve sketching, and is thus an appealing alternative to these 2D interfaces.

Our work is also related to drawing curves *around* surfaces. Such techniques are important for a variety of applications: modelling string and wire that wrap around objects [Coleman and Singh 2006]; curves that loosely conform to virtual objects [Krs et al. 2017]; clothing design on a 3D mannequin [Turquin et al. 2007]; layered modelling of shells and armour [De Paoli and Singh 2015]; and the design and grooming of hair and fur [Fu et al. 2007; Schmid et al. 2011; Xing et al. 2019]. Some approaches such as SecondSkin [De Paoli and Singh 2015] and Skippy [Krs et al. 2017] use insights into spatial relationship between a 2D stroke and the 3D object, to infer a 3D curve that lies on and around the surface of the object. Other techniques like Cords [Coleman and Singh 2006] or hair and clothing design [Xing et al. 2019] are closer to our work, in that they drape 3D curve input on and around 3D objects using geometric collisions or physical simulation. In contrast, this paper is focused on the general problem of projecting a drawn 3D stroke to a real-time inked curve on the surface of a 3D object. While we do not address curve creation with specific geometric relationships to the

object surface (like distance-offset curve), our techniques can be extended to incorporate geometry-specific terms (§ 8).

2.3 Sketch-based 3D Modelling

Sketch-based 3D modelling is a rich ongoing area of research (see survey by Olsen et al. [2009]). Typically, these systems interpret 2D sketch inputs for various shape modelling tasks. One could categorize these modelling approaches as single-view (akin to traditional pen on paper) [Andre and Saito 2011; Chen et al. 2013; Schmidt et al. 2009; Xu et al. 2014] or multi-view (akin to 3D modelling with frequent view manipulation) [Bae et al. 2008; Fan et al. 2013, 2004; Igarashi et al. 1999; Nealen et al. 2007]. Single-view techniques use perceptual insights and geometric properties of the 2D sketch to infer its depth in 3D, while multi-view techniques explicitly use view manipulation to specify 3D curve attributes from different views. While our work utilizes mid-air 3D stroke input, the ambiguity of projection onto surfaces connects it to the interpretative algorithms designed for sketch-based 3D modelling. We aim to take advantage of the immersive interaction space by allowing view manipulation as and when desired, independent of geometry creation.

3 PROJECTING STROKES ON 3D OBJECTS

We first formally state the problem of projecting a mid-air 3D stroke onto a 3D virtual object. Let $\mathcal{M} = (V, E, F)$ be a 3D object, represented as a manifold triangle mesh embedded in \mathbb{R}^3 . A user draws a piece-wise linear mid-air stroke by moving a 6-DoF controller or drawing tool in VR. The 3D stroke $\mathcal{P} \subset \mathbb{R}^3$ is a sequence of n points $(p_i)_{i=0}^{n-1}$, connected by line segments. Corresponding to each point $p_i \in \mathbb{R}^3$, is a system state $S_i = (h_i, c_i, h_i, c_i)$, where $h_i, c_i \in \mathbb{R}^3$ are the positions of the headset and the controller, respectively, and $h_i, c_i \in Sp(1)$ are their respective orientations, represented as unit quaternions. Also, without loss of generality, assume $c_i = p_i$, i.e. the controller positions describe the stroke points p_i .

We want to define a *projection* π , which transforms the sequence of points $(p_i)_{i=0}^{n-1}$ to a corresponding sequence of points $(q_i)_{i=0}^{n-1}$ on the 3D virtual object, i.e. $q_i \in \mathcal{M}$. Consecutive points in this sequence are connected by geodesics on \mathcal{M} , describing the *projected curve* $\mathcal{Q} \subset \mathcal{M}$. The aim of a successful projection method of course, is to match the undisclosed user-intended curve. The projection is also designed for real-time inking of curves: points p_i are processed upon input and projected in real-time (under 100ms) to q_i using the current system state S_i , and optionally, prior system states $(S_j)_{j=0}^{i-1}$, stroke points $(p_j)_{j=0}^{i-1}$ and projections $(q_j)_{j=0}^{i-1}$.

3.1 Context-Free Projection Techniques

Context-free techniques project points independent of each other, simply based on the spatial relationships between the controller, HMD, and 3D object (Figure 4). We can further categorize techniques as raycast or proximity based.

3.1.1 Raycast Projections. View-centric projection in 2D interfaces projects points from the screen along a ray from the eye through the screen point, to where the ray first intersects the 3D object. In an immersive setting, raycast approaches similarly use a ray emanating from the 3D stroke point to intersect 3D objects. This ray (o, d)

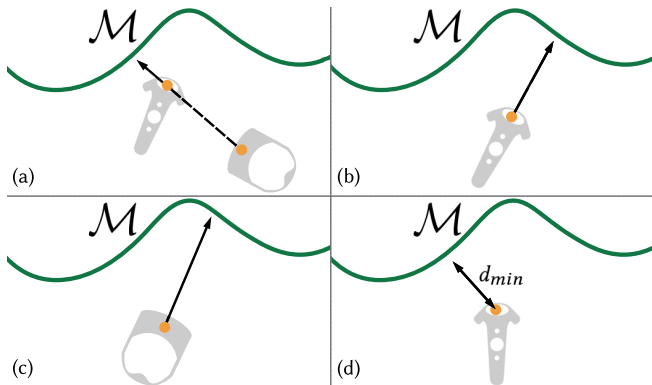


Fig. 4. Context-free techniques: *occlude* projects points from the controller origin along the direction from the eye (HMD origin) to the controller (a); *spraycan* projects points from the controller origin in a direction defined by the controller’s orientation (b); *head-centric*, akin to 2D projects points along the view direction defined by HMD orientation (c); *snap* projects points from the controller origin to their closest-point on \mathcal{M} (d).

with origin o and direction d can be defined in a number of ways. Similar to pointing behaviour, *occlude* defines this ray from the eye through the controller origin (Figure 4a) $(c_i, (c_i - h_i) / \|c_i - h_i\|)$. If the ray intersects \mathcal{M} , then the closest intersection to p_i defines q_i . In case of no intersection, p_i is ignored in defining the projected curve, i.e., q_i is marked undefined and the projected curve connects q_{i-1} to q_{i+1} (or the proximal index points on either side of i for which projections are defined). The *spraycan* approach treats the controller like a spraycan, defining the ray like a nozzle direction in the local space of the controller (Figure 4b). For example the ray could be defined as (c_i, f_i) , where the nozzle $f_i = c_i \cdot [0, 0, 1]^T$ is the controller’s local z-axis (or *forward* direction). Alternately, *head-centric* projection can define the ray using the HMD’s view direction as $(h_i, h_i \cdot [0, 0, 1]^T)$ (Figure 4c).

Pros and Cons: The strengths of raycasting are: a predictable visual/proprioceptive sense of ray direction; a spatially continuous mapping between user input and projection rays; and scenarios where it is difficult or undesirable to reach and draw close to the virtual object. Its biggest limitation stems from the controller/HMD-based ray direction being completely agnostic of the shape or location of the 3D object. Projected curves can consequently be very different in shape and size from drawn strokes (Figure 5a–b), and ill-defined for stroke points with no ray-object intersection.

3.1.2 Proximity-Based Projections. In 2D interfaces, the on-screen 2D strokes are typically distant to the viewed 3D scene, necessitating some form of raycast projection onto the visible surface of 3D objects. In AR/VR, however, users are able to reach out in 3D and directly draw the desired curve on the 3D object. While precise mid-air drawing on a virtual surface is very difficult in practice (Figure 3), projection methods based on proximity between the mid-air stroke and the 3D object are certainly worth investigation.

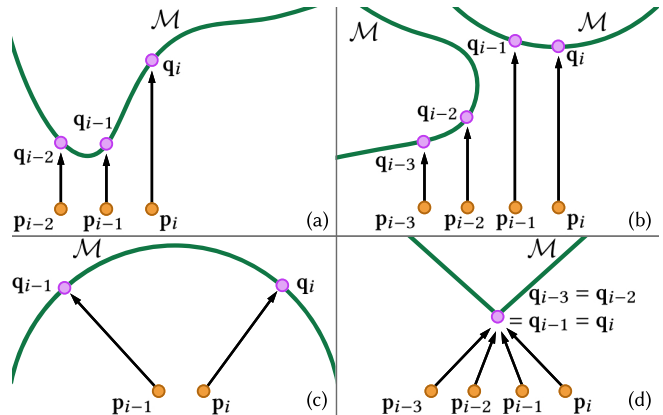
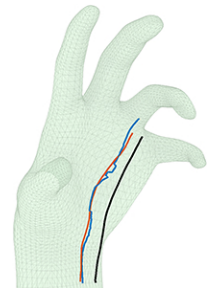


Fig. 5. Context-free projection problems: large depth disparity (a), unexpected jumps (b), projection discontinuities (c), and undesirable snapping (d).

The simplest proximity-based projection technique *snap*, projects a stroke point p_i to its closest-point in \mathcal{M} (Figure 4d).

$$q_i = \pi_{snap}(p_i) = \arg \min_{x \in \mathcal{M}} d(p_i, x), \quad (1)$$

where $d(\cdot, \cdot)$ is the Euclidean distance between two points. Unfortunately, for triangle meshes, closest-point projection tends to snap to mesh edges (blue curve inset), resulting in unexpectedly jaggy projected curves, even for smooth 3D input strokes (black curve inset) [Panozzo et al. 2013]. These discontinuities are due to the discrete nature of the mesh representation, as well as spatial singularities



in closest point computation even for smooth 3D objects. We mitigate this problem by formulating an extension of Panozzo et al.’s *Phong* projection [2013] in § 3.2, that simulates projection onto an imaginary smooth surface approximated by the mesh. We denote this *smooth-closest-point* projection as π_{SCP} (red curve inset).

Pros and Cons: The biggest strength of proximity-based projection is it exploits the immersive concept of drawing directly on or near an object, using the spatial relationship between a 3D stroke point and the 3D object to determine projection. The main limitation is that since users rarely draw precisely on the surface, discontinuities in concave regions (Figure 5c) and undesirable snapping in highly-convex regions (Figure 5d) persist when projecting distantly drawn stroke points, even when using *smooth-closest-point*. In § 4.1, we address this problem using stroke *mimicry* to anchor distant stroke points close to the object to be finally projected using *smooth-closest-point*.

3.2 Smooth-Closest-Point Projection

Our goal with *smooth-closest-point* projection is to define a mapping from a 3D point to a point on \mathcal{M} that approximates the closest point projection but tends to be functionally smooth, at least for points near the 3D object. We note that computing the closest point to a

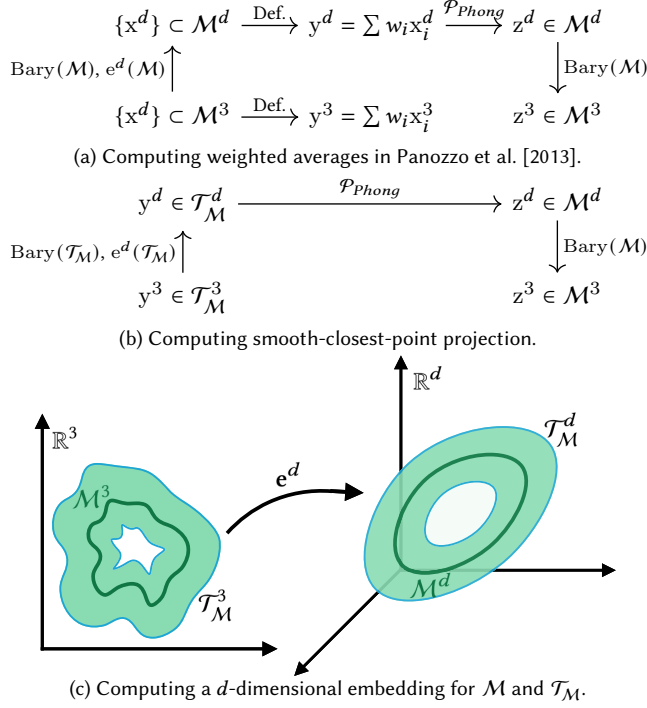


Fig. 6. Panozzo et al. [2013] compute weighted averages on surfaces (a), while we want to compute a smooth closest-point projection for an arbitrary point *near* the mesh in \mathbb{R}^3 (b). We therefore embed \mathcal{T}_M —the region around the mesh—in higher-dimensional space \mathbb{R}^d , instead of just \mathcal{M} (c).

Laplacian-smoothed mesh proxy, for example, will also provide a smoother mapping than π_{snap} , but a potentially poor closest-point approximation to the original mesh.

Phong projection, introduced by Panozzo et al. [2013], addresses these goals for points expressible as weighted-averages of points on \mathcal{M} , but we extend their technique to define a smooth-closest-point projection for points in the neighbourhood of the mesh. For completeness, we first present a brief overview of their technique.

Phong projection is a two-step approach to map a point $y^3 \in \mathbb{R}^3$ to a manifold triangle mesh \mathcal{M} embedded in \mathbb{R}^3 , emulating closest-point projection on a smooth surface approximated by the triangle mesh. First, \mathcal{M} is embedded in a higher dimensional Euclidean space \mathbb{R}^d such that Euclidean distance (between points on the mesh) in \mathbb{R}^d approximates geodesic distances in \mathbb{R}^3 . Second, analogous to vertex normal interpolation in Phong shading, a smooth surface is approximated by blending tangent planes across edges. Barycentric coordinates at a point within a triangle are used to blend the tangent planes corresponding to the three edges incident to the triangle. We extend the first step to a higher dimensional embedding of not just the triangle mesh \mathcal{M} , but a tetrahedral mesh of an offset volume around the mesh \mathcal{M} (Figure 6). The second step remains the same, and we refer the reader to Panozzo et al. [2013] for details. Such offset volumes, or *shells*, around triangle meshes have also been utilized in recent methods for curve design [Jin et al. 2019] and for attribute transfer between similar triangle meshes [Jiang et al. 2020].

For clarity, we refer to \mathcal{M} embedded in \mathbb{R}^3 as \mathcal{M}^3 , and the embedding in \mathbb{R}^d as \mathcal{M}^d . Panozzo et al. compute \mathcal{M}^d by first embedding a subset of the vertices in \mathbb{R}^D using metric multi-dimensional scaling (MDS) [Cox and Cox 2008], aiming to preserve the geodesic distance between the vertices. The embedding of the remaining vertices is then computed using LS-meshes [Sorkine and Cohen-Or 2004].

For the problem of computing weighted averages on surfaces, one only needs to project 3D points of the form $y^3 = \sum w_i x_i^3$, where all $x_i^3 \in \mathcal{M}^3$. The point y^3 is *lifted* into \mathbb{R}^d by simply defining $y^d = \sum w_i x_i^d$, where x_i^d is defined as the point on \mathcal{M}^d with the same implicit coordinates (triangle and barycentric coordinates) as x_i^3 does on \mathcal{M}^3 . Therefore, their approach only embeds \mathcal{M} into \mathbb{R}^d (Figure 6a,c). In contrast, we want to project arbitrary points *near* \mathcal{M}^3 onto it using the Phong projection. Therefore, we compute the offset surfaces at signed-distance $\pm\mu$ from \mathcal{M} . We then compute a tetrahedral mesh \mathcal{T}_M^3 of the space between these two surfaces in \mathbb{R}^3 . In the final precomputation step, we embed the vertices of \mathcal{T}_M in \mathbb{R}^d using MDS and LS-Meshes as described above.

Now, given a 3D point y^3 within a distance μ from \mathcal{M}^3 , we situate it within \mathcal{T}_M^3 , use tetrahedral Barycentric coordinates to infer its location in \mathbb{R}^d , and then compute its Phong projection (Figure 6b,c). We fallback to closest-point projection for points outside \mathcal{T}_M^3 , since Phong projection converges to closest-point projection when far from \mathcal{M} . Furthermore, we set μ large enough to easily handle our smooth-closest-point queries in § 4.1.

3.2.1 Projection Quality and Robustness Tests. Since the desirable properties of the Phong projection are not theoretically guaranteed for shapes with sharp features and noisy meshes [Panozzo et al. 2013], we experimentally measure the quality of the embedding by testing for extreme dihedral angles—below 5° or above 175° —resulting in sliver tets in the \mathbb{R}^d -embedding (Table 1). Further, for a direct measure of projection quality, we densely sampled points in \mathcal{T}_M (four points per tet) and projected each using both π_{snap} as well as π_{SCP} . Typically, we expect π_{SCP} to be a smoother version of π_{snap} (§ 3.1.2). Therefore, a π_{SCP} projection much farther from the input than π_{snap} indicates a clear failure:

$$\|p - \pi_{\text{SCP}}(p)\| > \|p - \pi_{\text{snap}}(p)\| + \|\text{BBox}(\mathcal{M}^3)\|/20, \quad (2)$$

where $\|\text{BBox}(\mathcal{M}^3)\|$ is the length of the bounding box diagonal of \mathcal{M}^3 . Table 1 shows that the projection works well for almost all the sampled points. We also practically tested all the shapes by drawing myriad curves on each, but did not notice any clear failures of π_{SCP} . Finally, we stress-tested the technique using noisy versions of the unit cube mesh. At extreme levels of noise, when each vertex is moved in the normal direction by up to 20% of the cube size, some clear failures showed up (Figure 17d). In practice, such failures can be detected heuristically and π_{snap} can be a drop-in replacement for such points. We, however, did not implement such a fix for our user study, or for the results shown in the paper.

3.3 Analysis of Context-Free Projection

We implemented the four different context-free projection approaches in Figure 4, and had 4 users informally test each, drawing a variety of curves on the various 3D models seen in this paper. The pilots

Table 1. Embedding quality and π_{SCP} failure results. The former is indicated by the percentage of dihedral angles $<5^\circ$ or $>175^\circ$ in the \mathbb{R}^d -embedding, and the latter is defined in Eq. 2 (lower values are desirable). Also shown are mesh sizes: (#vertices, #faces) for \mathcal{M} and (#vertices, #tets) for \mathcal{T}_M .

Shape	$ \mathcal{M} $	$ \mathcal{T}_M $	% slivers	% π_{SCP} fail
Trebol	(1.2K, 2.3K)	(7.9K, 38K)	6.89	0.00
Cube	(1.5K, 3.0K)	(5.7K, 26K)	17.44	< 0.01
Torus	(1.7K, 3.5K)	(11K, 58K)	0.41	0.00
Spiderman	(3.3K, 6.6K)	(15K, 83K)	2.01	0.02
Hand	(4.2K, 8.5K)	(19K, 114K)	0.49	0.39
Fertility	(4.5K, 9.0K)	(21K, 124K)	0.61	0.29
Fandisk	(6.5K, 13K)	(23K, 133K)	4.75	0.96
Bunny	(7.1K, 14K)	(32K, 183K)	4.17	0.08
Horse	(7.7K, 15K)	(34K, 198K)	0.41	0.35
La Madeleine	(20K, 40K)	(68K, 421K)	0.83	0.24
Beast	(30K, 61K)	(132K, 837K)	0.57	< 0.01
Armadillo	(50K, 100K)	(229K, 1.4M)	0.63	< 0.01
Noisy-cube 5%	(1.5K, 3.0K)	(29K, 139K)	35.78	< 0.01
Noisy-cube 10%	(1.5K, 3.0K)	(30K, 149K)	30.07	0.05
Noisy-cube 15%	(1.5K, 3.0K)	(33K, 164K)	21.08	0.93
Noisy-cube 20%	(1.5K, 3.0K)	(33K, 167K)	10.95	3.73

helped understand the limitations of context-free projections, as noted in Section 3.1 and illustrated in Figure 5. Additional details about the pilot observations are given in Appendix A.

The most valuable insight was that the user stroke in mid-air often tended to **mimic** the expected projected curve. Context-free approaches, by design, are unable to capture this mimicry, i.e., the notion that the change between projected point as we draw a stroke is commensurate with the change in the 3D points along the stroke. This observation motivated us to design projection methods that explicitly incorporate the shape of the mid-air stroke \mathcal{P} and the projected curve \mathcal{Q} . We call these functions *anchored*.

4 ANCHORED STROKE PROJECTION

The limitations of context-free projection can be addressed by equipping stroke point projection with the context/history of recently drawn points and their projections. In this paper we minimally use only the most recent stroke point p_{i-1} and its projection q_{i-1} , as context to **anchor** the current projection.

Any reasonable context-free projection can be used for the first stroke point p_0 . We use *spraycan* π_{spray} , our preferred context-free technique. For subsequent points ($i > 0$), we compute:

$$r_i = q_{i-1} + \Delta p_i, \quad (3)$$

where $\Delta p_i = (p_i - p_{i-1})$. We then compute q_i as a projection of the anchored stroke point r_i onto \mathcal{M} , that attempts to capture $\Delta p_i \approx \Delta q_i$. Anchored projection captures our observation that the mid-air user stroke tends to **mimic** the shape of their intended curve on surface. While users do not adhere consciously to any precise geometric formulation of mimicry, we observe that users often draw the intended projected curve as a corresponding stroke

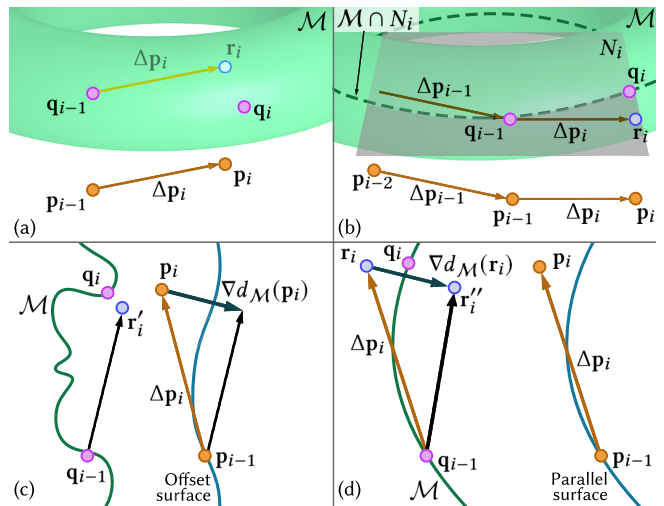


Fig. 7. Anchored smooth-closest-point (a), and refinements: using a locally-fit plane (b), and anchor point constrained to an offset (c) or parallel surface (d). q_i is obtained by projecting r_i (a), r'_i (c), or r''_i (d) onto \mathcal{M} via smooth-closest-point; or closest-point to r_i in $\mathcal{M} \cap N_i$ (b).

on an imagined offset or translated surface (Figure 7). A good general projection for the anchored point r_i to \mathcal{M} thus needs to be continuous, predictable, and loosely capture this notion of mimicry.

4.1 Mimicry Projection

Controller sampling rate in current VR systems is 50Hz or more, meaning that even during ballistic movements, the distance $\|\Delta p_i\|$ for any stroke sample i is of the order of a few millimetres. Consequently, the anchored stroke point r_i is typically much closer to \mathcal{M} , than the stroke point p_i , making closest-point *snap* projection a compelling candidate for projecting r_i . Such an *anchored closest-point* projection explicitly minimizes $\|\Delta p_i - \Delta q_i\|$, but precise minimization is less important than avoiding projection discontinuities and undesirably snapping, even for points close to the mesh. Our formulation of a *smooth-closest-point* projection π_{SCP} in § 3.2 addresses these goals precisely. We define *mimicry* projection as

$$\Pi_{mimicry}(p_i) = \begin{cases} \pi_{spray}(p_i) & \text{if } i = 0, \\ \pi_{SCP}(r_i) & \text{otherwise.} \end{cases} \quad (4)$$

4.2 Refinements to Mimicry Projection

We further explore refinements to *mimicry* projection, that might improve curve projection in certain scenarios.

Planar curves are very common in design and visualization [McCrae et al. 2011]. We can locally encourage planarity in mimicry projection by constructing a plane N_i with normal $\Delta p_i \times \Delta p_{i-1}$ (i.e. the local plane of the mid-air stroke) and passing through the anchor point r_i (Figure 7b). We then intersect N_i with \mathcal{M} . q_i is defined as the closest-point to r_i on the intersection curve that contains q_{i-1} . Note, we use $\pi_{spray}(p_i)$ for $i < 2$, and we retain the most recently defined normal direction (N_{i-1} or prior) when $N_i = \Delta p_i \times \Delta p_{i-1}$ is undefined. We find this method works well for near-planar curves,

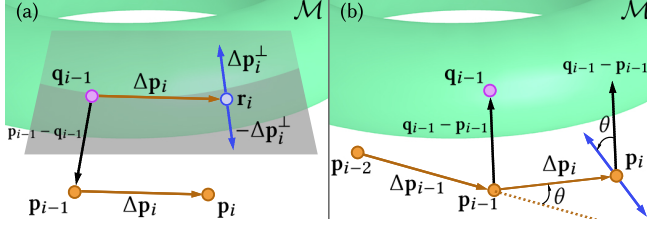


Fig. 8. Anchored raycast techniques: ray direction defined orthogonal to Δp_i in a local plane (a); parallel transport of ray direction along the user stroke (b). The cast rays (forward/backward) are shown in blue.

but the plane is sensitive to noise in the mid-air stroke (Figure 9f), and can feel *sticky* or less responsive for non-planar curves.

Offset and parallel surface drawing captures the observation that users tend to draw an intended curve as a corresponding stroke on an imaginary offset or parallel surface of the object \mathcal{M} . While we do not expect users to draw precisely on such surfaces, it is unlikely a user would intentionally draw orthogonal to them.

In scenarios when a user is sub-consciously drawing on an offset surface of \mathcal{M} (an isosurface of its signed-distance function $d_{\mathcal{M}}(\cdot)$), we can remove the component of a user stroke segment along the gradient $\nabla d_{\mathcal{M}}$, when computing the anchor point (Figure 7c):

$$r'_i = q_{i-1} + \Delta p_i - \left(\Delta p_i \cdot \nabla d_{\mathcal{M}}(p_i) \right) \nabla d_{\mathcal{M}}(p_i) \quad (5)$$

We can similarly locally constrain user strokes to a parallel surface of \mathcal{M} in Equation 6 as:

$$r''_i = q_{i-1} + \Delta p_i - \left(\Delta p_i \cdot \nabla d_{\mathcal{M}}(r_i) \right) \nabla d_{\mathcal{M}}(r_i). \quad (6)$$

Note that the difference from Eq. 5 is the position where $\nabla d_{\mathcal{M}}$ is computed, as shown in Figure 7d. A parallel surface better matched user expectation than an offset surface in our pilot testing, but both techniques produced poor results when user drawing deviated from these imaginary surfaces (Figure 9g-l).

4.3 Anchored Raycast Projection

For completeness, we also investigated raycast alternatives to projection of the anchored stroke point r_i . We used similar priors of local planarity and offset or parallel surface transport as with mimicry refinement, to define ray directions. Figure 8 shows two such options.

In Figure 8a, we cast a ray in the local plane of motion, orthogonal to the user stroke, given by Δp_i . We construct the local plane containing r_i spanned by Δp_i and $p_{i-1} - q_{i-1}$, and then define the direction orthogonal to Δp_i in this plane. Since r_i may be inside \mathcal{M} , we cast two rays bi-directionally ($r_i, \pm \Delta p_i^\perp$), where

$$\Delta p_i^\perp = \Delta p_i \times (\Delta p_i \times (p_{i-1} - q_{i-1}))$$

If both rays successfully intersect \mathcal{M} , we choose q_i to be the point closer to r_i . As with locally planar mimicry projection, this technique suffered from instability in the local plane.

Motivated by mimicry, we also explored parallel transport of the projection ray direction along the user stroke (Figure 8b). For $i > 0$, we parallel transport the previous projection direction $q_{i-1} - p_{i-1}$ along the mid-air curve by rotating it with the rotation that aligns

Δp_{i-1} with Δp_i . Once again, bi-directional rays are cast from r_i , and q_i is set to the closer intersection with \mathcal{M} .

In general, we found that all raycast projections, even when anchored, suffered from unpredictability over long strokes and discontinuities when there are no ray-object intersections (Figure 9n,o).

4.4 Final Analysis and Implementation Details

In summary, extensive pilot testing of the anchored techniques revealed that they were generally better than context-free approaches, especially when users drew further away from the 3D object. Among anchored techniques, stroke mimicry captured as an *anchored-smooth-closest-point* projection proved to be theoretically elegant, and practically the most resilient to ambiguities of user intent and differences of drawing style among users. *Anchored closest-point* can be a reasonable proxy to *anchored smooth-closest-point* when pre-processing is undesirable. A pertinent application is real-time sculpting, where the object shape changes frequently.

Our techniques are implemented in C#, with interaction, rendering, and VR support provided by the Unity Engine. For the smooth closest-point operation, we modified Panozzo et al.'s [2013] reference implementation, which includes pre-processing code in MATLAB and C++, and real-time code in C++. The real-time projection implementation is exposed to our C# application via a compiled dynamic library. In their implementation, as well as ours, $d = 8$; that is, we embed \mathcal{M} in \mathbb{R}^8 . Offset surfaces are computed using libigl [Jacobson et al. 2018], with $\mu = \|\text{BBox}(\mathcal{M})\|/20$. We then improve surface quality using TetWild [Hu et al. 2018], before computing the tetrahedral mesh $\mathcal{T}_{\mathcal{M}}$ using TetGen [Si 2015].

We support fast closest-point queries, using an AABB tree implemented in geometry3Sharp [Schmidt 2017]. Signed-distance is also computed using the AABB tree and fast winding number [Barill et al. 2018], and gradient $\nabla d_{\mathcal{M}}$ computed using central finite differences.

To ease replication of our various techniques and aid future work, we have released our open-source implementation at github.com/rarora7777/curve-on-surface-drawing-vr.

We now formally compare our most promising projection *mimicry*, to the best state-of-the-art context-free projection *sprayscan*.

5 USER STUDY

We designed a user study to compare the performance of the *sprayscan* and *mimicry* methods for a variety of curve-drawing tasks. We selected six shapes for the experiment (Figure 10), aiming to cover a diverse range of shape characteristics: sharp features (*cube*), large smooth regions (*trebol*, *bunny*), small details with ridges and valleys (*bunny*), thin features (*hand*), and topological holes (*torus*, *fertility*).

We then sampled ten distinct curves on the surface of each of the six objects. A canonical task in our study involved the participant attempting to re-create a given *target curve* from this set. We designed two types of drawing tasks shown in Figure 11:

Tracing curves, where a participant tried to trace over a visible target curve using a single smooth stroke.

Re-creating curves, where a participant attempted to re-create from memory, a visible target curve that was hidden as soon as the participant started to draw. An enumerated set of keypoints on the

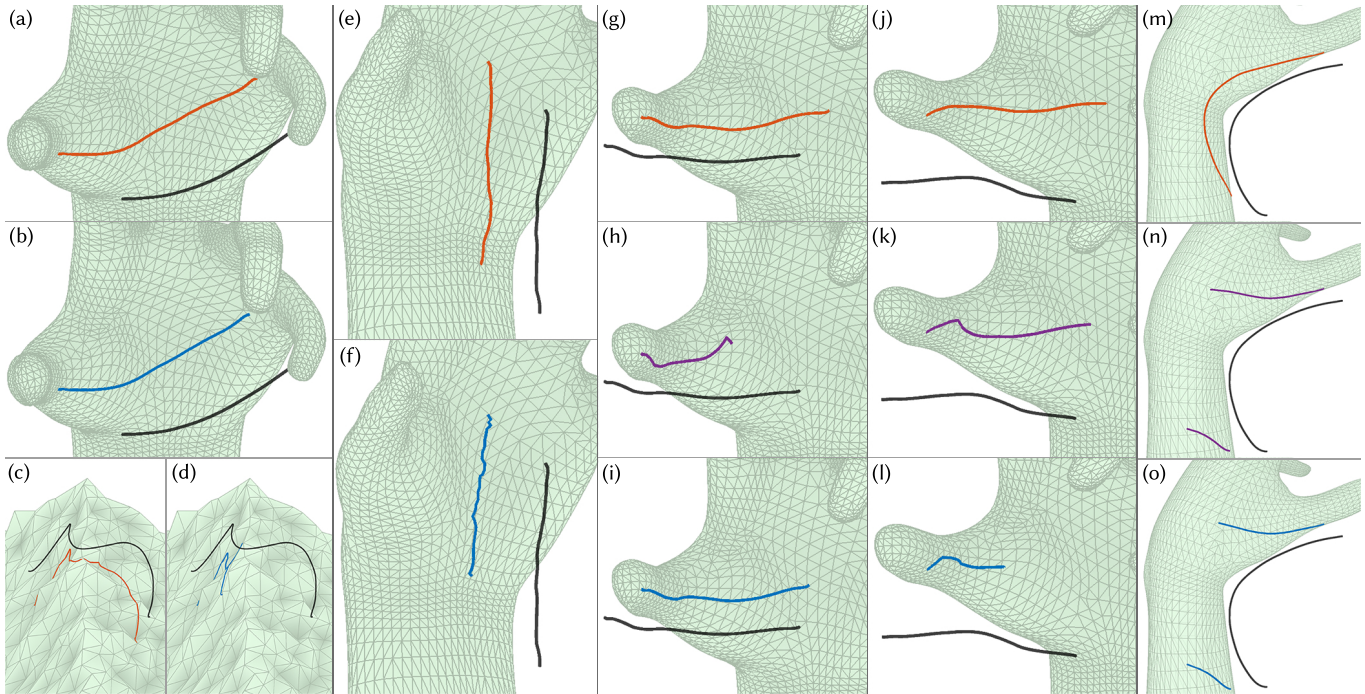


Fig. 9. *Mimicry* vs. other anchored stroke projections: Mid-air strokes are shown in **black** and *mimicry* curves in **red**. Anchored closest-point (**blue**), is similar to *mimicry* on smooth, low-curvature meshes (a,b) but degrades with mesh detail/noise (c,d). Locally planar projection (**blue**) is susceptible local plane instability (e,f). Parallel (**purple** h,k) or offset (**blue** i,l) surface based projection fail in (h,l) when the user stroke deviates from said surface, while *mimicry* remains reasonable (g, j). Compared to *mimicry* (m), anchored raycasting based on a local plane (**purple** n), or ray transport (**blue** o) can be discontinuous.

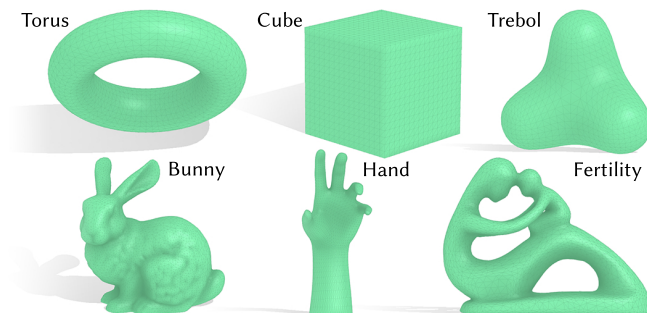


Fig. 10. The six shapes utilized in the user study. The *torus* shape was used for tutorials, while the rest were used for the recorded experimental tasks.

curve, however, remained as a visual reference, to aid the participant in re-creating the hidden curve with a single smooth stroke.

The rationale behind asking users to draw target curves is both to control the length, complexity, and nature of curves drawn by users, and to have an explicit representation of the user-intended curve. Curve tracing and re-creating are fundamentally different drawing tasks, each with important applications [Arora et al. 2017]. Our curve re-creation task is designed to capture free-form drawing, with minimal visual suggestion of intended target curve.

Target curves were sampled randomly from a distribution of long, smooth, curves on the mesh. For each sample curve, 4–9 keypoints

were selected along endpoints and curvature extrema, the number depending on the curve’s length and complexity. Positioning keypoints at curvature extrema ensured that curve re-creating tasks amounted to smoothly joining the keypoints, rather than testing participants’ memory. Appendix B provides details about the sampling process.

5.1 Experiment Design

The main variable studied in the experiment was *Projection method—spraycan vs. mimicry*—realized as a within-subjects variable. The order of methods was counterbalanced between participants. For each method, participants were exposed to all the six objects. Object order was fixed as torus, cube, trebol, bunny, hand, and fertility, based on our personal judgment of drawing difficulty. The torus was used as a tutorial, where participants had access to additional instructions visible in the scene and their strokes were not utilized for analysis. For each object, the order of the 10 target strokes was randomized. The first five were used for the tracing curves task, while the remaining five were used for re-creating curves.

The target curve for the first tracing task was repeated after the five unique curves, to gauge user consistency and learning effects. A similar repetition was used for curve re-creation. Participants thus performed 12 curve drawing tasks per object, leading to a total of 12×5 (objects) $\times 2$ (projections) = 120 strokes per participant.

Owing to the COVID-19 physical distancing guidelines, the study was conducted on participants’ personal VR equipment at their

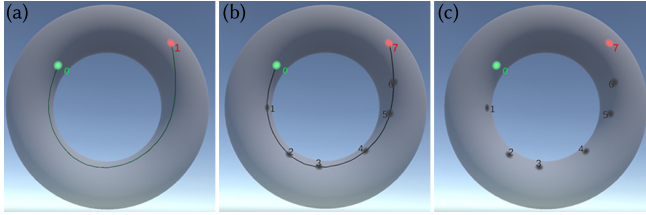


Fig. 11. Study tasks—*curve tracing*: target curve is visible when drawing (a), and *curve re-creation*: target curve (b) is hidden when drawing (c).

homes. A 15-minute instruction video introduced the study tasks and the two projection methods. Participants then filled out a consent form and a questionnaire to collect demographic information. This was followed by them testing the first projection method and filling out a questionnaire to express their subjective opinions of the method. They then tested the second method, followed by a similar questionnaire, and questions involving subjective comparisons between the two methods. Participants were required to take a break after testing the first method, and were also encouraged to take breaks after drawing on the first three shapes for each method. The study took approximately an hour, including the questionnaires.

5.2 Participants

Twenty participants (5 female, 15 male) aged 21–47 from five countries participated in the study. All but one were right-handed. Participants were not selected for artistic ability or prior VR experience, and exhibited a diverse range of self-reported artistic abilities (min. 1, max. 5, median 3 on a 1–5 scale) as well as varying degrees of VR experience, ranging from below 1 year to over 5 years. 13 participants had a technical computer graphics or HCI background, while ten had experience with creative tools in VR, with one reporting professional usage. Participants were paid ≈ 22 USD as a gift card.

5.3 Apparatus

As the study was conducted on personal VR setups, a variety of commercial VR devices were utilized—Oculus Rift, Rift S, and Quest using Link cable, HTC Vive and Vive Pro, Valve Index, and Samsung Odyssey using Windows Mixed Reality. All but one participant used a standing setup allowing them to freely move around.

5.4 Procedure

Before each trial, participants could use the “grab” button on their controller (in the dominant hand) to grab the mesh to position and orient it as desired. The trial started as soon as the participant started to draw by pressing the “main trigger” on their dominant hand controller. This action disabled the grabbing interaction—participants could not draw and move the object simultaneously. As noted earlier, for curve re-creation tasks, this had the additional effect of hiding the target curve, but leaving keypoints visible.

6 STUDY RESULTS AND DISCUSSION

We recorded the head position h and orientation h , controller position c and orientation c , projected point q , and timestamp t , for

each mid-air stroke point $p = c$. We refer to a target curve as \mathcal{X} , a mid-air stroke as \mathcal{P} , and a projected curve as \mathcal{Q} .

6.1 Data Processing and Filtering

We formulated three criteria to filter out meaningless user strokes.

Short Curves. We ignore projected curves \mathcal{Q} that are too short as compared to the length of the target curves \mathcal{X} (conservatively curves less than half as long as the target curve). While it is possible that the user stopped drawing mid-way out of frustration, we found it was more likely that they prematurely released the controller trigger by accident. Both curve lengths are computed in \mathbb{R}^3 for efficiency.

Stroke Noise. We ignore strokes for which the mid-air stroke is too noisy. Specifically, mid-air strokes with distant consecutive points ($\exists i$ s.t. $\|p_i - p_{i-1}\| > 5\text{cm}$) are rejected.

Inverted Curves. While we labelled keypoints with numbers and marked start and end points in green and red (Figure 11), some users occasionally drew the target curve in reverse. The motion to draw a curve in reverse is not symmetric, and such curves are thus rejected. We detect inverted strokes by looking at the indices i_0, i_1, \dots, i_l of the points in \mathcal{Q} which are closest to the keypoints $x_{k_0}, x_{k_1}, \dots, x_{k_l}$ of \mathcal{X} . Ideally, the sequence i_0, \dots, i_l should have no inversions, i.e., $\forall 0 \leq j < k \leq l, i_j \leq i_k$; and maximum $l(l+1)/2$ inversions, if \mathcal{Q} is aligned in reverse with \mathcal{X} . We consider curves with more than $l(l+1)/4$ (half the maximum) inversions to be inadvertently inverted and reject them. Distances are computed in \mathbb{R}^3 for efficiency.

Despite conducting our experiment remotely without supervision, we found that 95.8% of the strokes satisfied our criteria and could be utilized for analysis. Out of the 102 strokes deemed unfit for analysis, 17 were too short, 66 were inverted, and 38 exhibited excessive tracking noise. It is possible that some of the short or inverted curves were caused due to curve control issues, there is no robust automatic method for distinguishing between inadvertent errors and genuine challenges faced by the users. Given the small number of such strokes and the potential bias in manual classification, we chose to exclude these strokes from the analysis. For comparisons between π_{spray} and π_{mimicry} , we reject stroke pairs where either stroke did not satisfy the quality criteria. Out of 1200 pairs (2400 total strokes), 1103 (91.9%) satisfied the quality criteria and were used for analysis, including 564 pairs for the curve re-creation task and 539 for the tracing task.

6.2 Quantitative Analysis

We define 10 different statistical measures (Table 2) to compare π_{spray} and π_{mimicry} curves in terms of their accuracy, aesthetic, and effort in curve creation. We consistently use the non-parametric Wilcoxon signed rank test for all quantitative measures instead of a parametric test such as the paired t -test, since the recorded data for none of our measures was normally distributed (normality hypothesis rejected via the Kolmogorov-Smirnov test, $p < .005$). In addition, we analyze users’ tendency to mimic the target strokes and consistency between repeated strokes in Appendix C.

6.2.1 Curve Accuracy. Accuracy is computed using two measures of distance between points on the projected curve \mathcal{Q} and target

Table 2. Quantitative results (mean \pm std. dev.) of the comparisons between *mimicry* and *spraycan* projection. All measures are analyzed using Wilcoxon signed-rank tests, lower values are better, and significantly better values ($p < .05$) are shown in **boldface**. Accuracy, aesthetic, and physical effort measures are shown with green, red, and blue backgrounds, respectively.

TRACING CURVES				
Measure	Spraycan	Mimicry	<i>p</i> -value	<i>z</i> -stat
D_{ep}	2.31 \pm 2.64 mm	1.13 \pm 1.11 mm	<.001	8.36
D_{sym}	0.64 \pm 0.66 mm	0.56 \pm 0.44 mm	>.05	-0.09
K_E	280 \pm 262 rad/m	174 \pm 162 rad/m	<.001	15.59
K_g	249 \pm 245 rad/m	152 \pm 157 rad/m	<.001	15.42
F_g	394 \pm 413 rad/m	248 \pm 285 rad/m	<.001	14.82
T_h	0.81 \pm 0.70	0.58 \pm 0.40	<.001	7.93
R_h	1.63 \pm 2.18 rad/m	1.18 \pm 1.63 rad/m	<.001	4.82
T_c	1.05 \pm 0.36	1.10 \pm 0.29	<.001	-3.36
R_c	5.12 \pm 5.88 rad/m	3.79 \pm 4.84 rad/m	<.001	5.51
τ	4.69 \pm 1.85 s	5.29 \pm 2.17 s	<.001	-7.32
RE-CREATING CURVES				
Measure	Spraycan	Mimicry	<i>p</i> -value	<i>z</i> -stat
D_{ep}	2.34 \pm 2.49 mm	2.24 \pm 23.32 mm	<.001	8.63
D_{sym}	0.75 \pm 0.65 mm	1.12 \pm 11.51 mm	>.05	0.55
K_E	254 \pm 236 rad/m	155 \pm 127 rad/m	<.001	14.70
K_g	223 \pm 219 rad/m	132 \pm 123 rad/m	<.001	14.95
F_g	348 \pm 371 rad/m	215 \pm 227 rad/m	<.001	14.11
T_h	0.72 \pm 0.54	0.54 \pm 0.35	<.001	6.78
R_h	1.50 \pm 2.19 rad/m	1.32 \pm 1.99 rad/m	.002	3.07
T_c	1.05 \pm 0.37	1.11 \pm 0.23	<.001	-5.94
R_c	5.23 \pm 6.36 rad/m	3.63 \pm 5.13 rad/m	<.001	4.00
τ	4.33 \pm 1.57 s	4.92 \pm 1.89 s	<.001	-7.12

curve \mathcal{X} . Both curves are densely re-sampled using $m = 101$ sample points equi-spaced by arc-length.

Given $Q = q_0, \dots, q_{m-1}$ and $\mathcal{X} = x_0, \dots, x_{m-1}$, we compute the *average equi-parameter distance* D_{ep} as

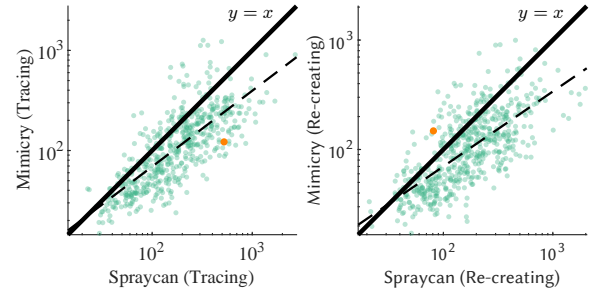
$$D_{ep}(Q) = \frac{1}{m} \sum_{i=0}^{m-1} d_E(q_i, x_i), \quad (7)$$

where d_E computes the Euclidean distance between two points in \mathbb{R}^3 . We also compute the *average symmetric distance* D_{sym} as

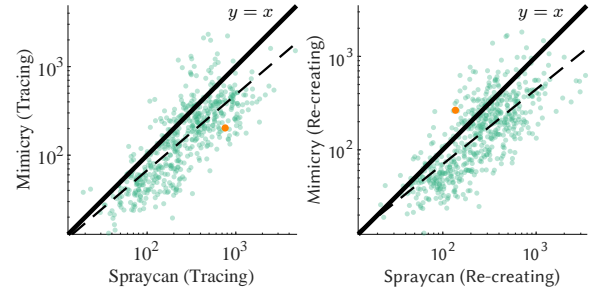
$$D_{sym}(Q) = \frac{1}{2m} \sum_{i=0}^{m-1} \left(\min_{x \in \mathcal{X}} d_E(q_i, x) \right) + \frac{1}{2m} \sum_{i=0}^{m-1} \left(\min_{q \in Q} d_E(x, q) \right)$$

In other words, D_{ep} computes the distance between corresponding points on the two curves and D_{sym} computes the average minimum distance from each point on one curve to the other curve.

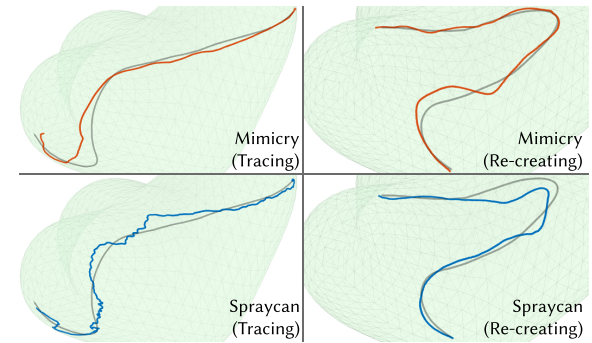
For both tracing and re-creation tasks, D_{ep} indicated that *mimicry* produced significantly better results than *spraycan* (see Table 2, Figure 1c, 12). The D_{sym} difference was not statistically significant, evidenced by users correcting their strokes to stay close to the intended target curve (at the expense of curve aesthetic).



(a) Normalized geodesic curvature K_g .



(b) Normalized fairness deficiency F_g .



(c) Example strokes, orange points in (a, b) above.

Fig. 12. Curvature measures (a,b) indicate that *mimicry* produces significantly smoother and fairer curves than *spraycan* for both tracing (left) and re-creating tasks (right). Pairwise comparison plots between *mimicry* (*y*-axis) and *spraycan* (*x*-axis), favour *mimicry* for the vast majority of points (points below the $y = x$ line). A linear regression fit (on the log plots) is shown as a dashed line. Example curve pairs (orange points) for curve tracing and re-creating are also shown with the target curve \mathcal{X} shown in gray (c).

6.2.2 Curve Aesthetic. For most design applications, jagged projected curves, even if geometrically quite accurate, are aesthetically undesirable [McCrae and Singh 2008]. Curvature-based measures are typically used to measure fairness of curves. We report three such measures of curve aesthetic for the projected curve $Q = q_0, \dots, q_{n-1}$. We first refine Q by computing the exact geodesic on \mathcal{M} between consecutive points of Q [Surazhsky et al. 2005], to create \hat{Q} with points $\hat{q}_0, \dots, \hat{q}_{k-1}$, $k \geq n$. We choose to normalize our curvature measures using $L_{\mathcal{X}}$, the length of the corresponding target stroke \mathcal{X} . The *normalized Euclidean curvature* for

Q is defined as

$$K_E(Q) = \frac{1}{L_X} \sum_{i=1}^{k-2} \theta_i \quad (8)$$

where θ_i is the angle between the two segments of \widehat{Q} incident on \widehat{q}_i . Thus, K_E is the total discrete curvature of \widehat{Q} , normalized by the target curve length.

Since \widehat{Q} is embedded in \mathcal{M} , we can also compute discrete *geodesic* curvature, computed as the deviation from the straightest geodesic on a surface. Using a signed θ_i^g defined at each point \widehat{q}_i [Polthier and Schmieß 2006], we compute *normalized geodesic curvature* as

$$K_g(Q) = \frac{1}{L_X} \sum_{i=1}^{k-2} |\theta_i^g|. \quad (9)$$

Finally, we define *fairness* [Arora et al. 2017; McCrae and Singh 2008] as a first-order variation in geodesic curvature, thus defining the *normalized fairness deficiency* as

$$F_g(Q) = \frac{1}{L_X} \sum_{i=2}^{k-2} |\theta_i^g - \theta_{i-1}^g|. \quad (10)$$

For all three measures, a lower value indicates a smoother, pleasing, curve. Wilcoxon signed-rank tests on all three measures indicated that *mimicry* produced significantly smoother and better curves than *spraycan* (Table 2).

6.2.3 Physical Effort. The amount of head (HMD) and hand (controller) movement, and stroke *execution time* τ provide quantitative proxies for physical effort.

For head and hand translation, we first filter the position data with a Gaussian-weighted moving average filter with $\sigma = 20$ ms. We then define *normalized head/controller translation* T_h and T_c as the length of the poly-line defined by the filtered head/controller positions normalized by the length of the target curve L_X .

An important ergonomic measure is the amount of head/hand rotation required to draw the mid-air stroke. We first de-noise or filter the forward and up vectors of the head/controller frame, using the same filter as for positional data. We then re-orthogonalize the frames and compute the length of the curve defined by the filtered orientations in $SO(3)$, using the angle between consecutive orientation data-points. We define *normalized head/controller rotation* R_h and R_c as its orientation curve length, normalized by L_X .

Table 2 summarizes the physical effort measures. We observe lower controller translation (effect size $\approx 5\%$) and execution time (effect size $\approx 12\%$) in favour of *spraycan*; lower head translation and orientation (effect sizes $\approx 36\%$, 26%) in favour of *mimicry*. Noteworthy is the significantly reduced controller rotation using *mimicry*, with *spraycan* unsurprisingly requiring 35% (tracing) and 44% (re-creating) more hand rotation from the user.

6.3 Qualitative Analysis

The mid- and post-study questionnaires elicited qualitative responses from participants on their perceived difficulty of drawing, curve accuracy and smoothness, mental and physical effort, understanding of the projection methods, and overall method of preference.

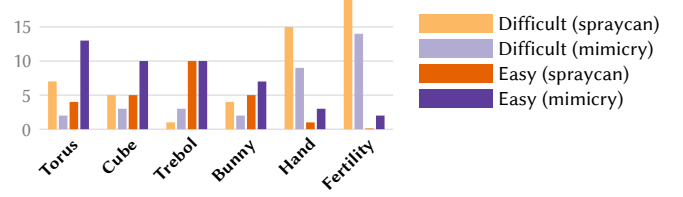
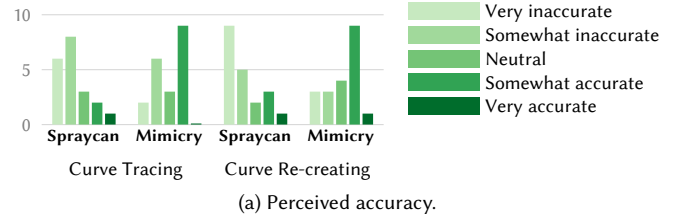
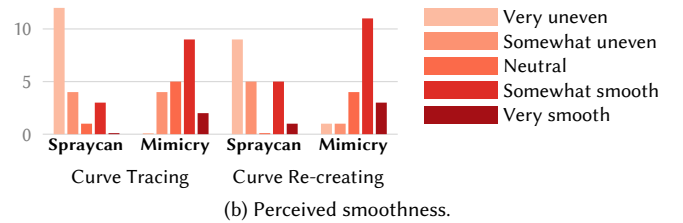


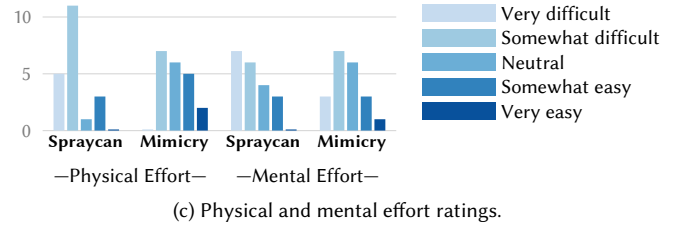
Fig. 13. Perceived difficulty of drawing for the six 3D shapes in the study.



(a) Perceived accuracy.



(b) Perceived smoothness.



(c) Physical and mental effort ratings.

Fig. 14. Participants perceived *mimicry* to be better than *spraycan* in terms of accuracy (a), curve aesthetic (b) and user effort (c).

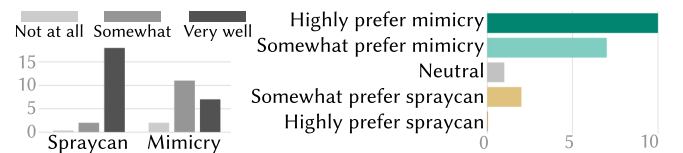


Fig. 15. Participants stated understanding *spraycan* projection better (left); 17/20 users stated an overall preference for *mimicry* over *spraycan* (right).

Participants were asked to specify the objects which they found especially easy or difficult to draw on, when using either of the two projection methods. In general, the shapes shown earlier were judged to be easier to work with (Figure 13), validating our ordering of shapes in the experiment based on expected drawing difficulty. Importantly, this observation also suggests a lack of any learning effects caused by the fixed object ordering.

Accuracy, smoothness, physical/mental effort responses were collected via 5-point Likert scales. We consistently order the choices

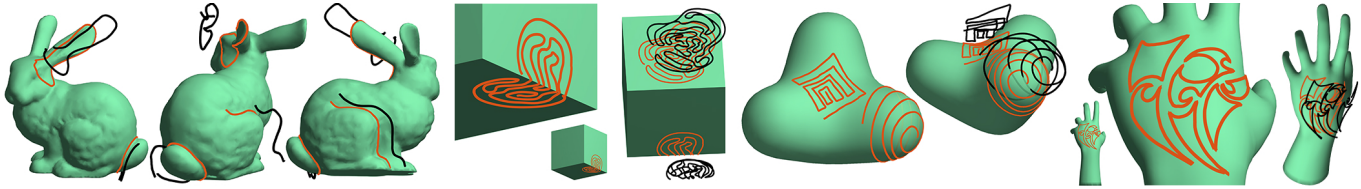


Fig. 16. Gallery of free-form curves in red, drawn by the paper authors using *mimicy*. (Left to right) tracing geometric features on the bunny, maze-like curves on the cube, maze with sharp corners and a spiral on the treble, and artistic tattoo motifs on the hand. Some mid-air strokes (black) hidden for clarity.

from 1 (worst) to 5 (best) in terms of user experience, and report median (M) scores here. *Mimicy* was perceived to be a more accurate projection (tracing, re-creating $M = 3, 3.5$) compared to *spraycan* ($M = 2, 2$), with 9 participants perceiving their traced curves to be either *very accurate* or *somewhat accurate* with *mimicy*, compared to 2 for *spraycan* (Figure 14a). Perception of stroke smoothness was also consistent with quantitative results, with *mimicy* (tracing, re-creating $M = 4, 4$) clearly outperforming *spraycan* (tracing, re-creating $M = 1, 2$) (Figure 14b). Lastly, with no need for controller rotation, *mimicy* ($M = 3$) was perceived as less physically demanding than *spraycan* ($M = 2$), as expected (Figure 14c).

The response to understanding and mental effort was more complex. *Spraycan*, with its physical analogy and mathematically precise definition was clearly understood by all 20 participants (17 very well, 3 somewhat) (Figure 15a). *Mimicy*, conveyed as “drawing a mid-air stroke on or near the object as similar in shape as possible to the intended projection”, was less clear to users (7 very well, 11 somewhat, 3 not at all). Despite not understanding the method consciously, the 3 participants were able to create curves that were both accurate and smooth. Further, users perceived *mimicy* ($M = 2.5$) as less cognitively taxing than *spraycan* ($M = 2$) (Figure 14c). We believe this may be because users were less prone to consciously controlling their stroke direction and rather focused on drawing. The tendency to mimic may have thus manifested sub-consciously, as we had observed in pilot testing.

The most important qualitative question was user preference (Figure 15b). 85% of the 20 participants preferred *mimicy* (10 highly preferred, 7 somewhat preferred). The remaining users were neutral (1/20) or somewhat preferred *spraycan* (2/20).

6.4 Participant Feedback

We also asked participants to elaborate on their stated preferences and ratings. Participants ($P4, 8, 16, 17$) noted discontinuous “jumps” caused by *spraycan*, and felt the continuity guarantee of *mimicy*: “seemed to deal with the types of jitter and inaccuracy VR setups are prone to better” ($P6$); “could stabilize my drawing” ($P9$). $P9, 15$ felt that *mimicy* projection was smoothing their strokes (no smoothing was employed): we believe this may be the effect of noise and inadvertent controller rotation, which *mimicy* ignores, but can cause large variations with *spraycan*, perceived as curve smoothing.

Some participants ($P4, 17$) felt that rotating the hand smoothly while drawing was difficult, while others missed the *spraycan* ability to simply use hand rotation to sweep out long projected curves from a distance ($P2, 7$). Participants commented on physical effort:

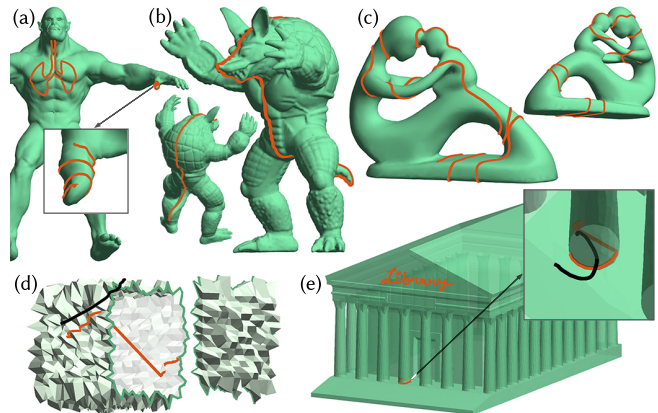


Fig. 17. *Mimicy* can be used to draw long, complicated curves on complex high-resolution meshes. We show strokes on high-resolution meshes (a, b, e), a long stroke bisecting a model (b), and a single stroke winding around a topologically non-trivial object multiple times (c). However, excessive noise in the input mesh can break the underlying π_{ACP} assumptions, resulting in catastrophic failure (d). Mesh has been cut open for visualization. Large meshes with many sharp features and topological complexity can also show smaller local failures in the form of unexpected jumps when drawing close to the sharp features (e, inset).

“*Mimicy* method seemed to required [sic] much less head movement, hand rotation and mental planning” ($P4$).

Participants appreciated the anchored control of *mimicy* in high-curvature regions ($P1, 2, 4, 8$) also noting that with *spraycan*, “the curvature of the surface could completely mess up my stroke” ($P1$). Some participants did feel that *spraycan* could be preferable when drawing on near-flat regions of the mesh ($P3, 14, 19, 20$).

Finally, participants who preferred *spraycan* felt that *mimicy* required more thinking: “with *mimicy*, there was extra mental effort needed to predict where the line would go on each movement” ($P3$), or because *mimicy* felt “unintuitive” ($P7$) due to their prior experience using a *spraycan* technique. Some who preferred *mimicy* found it difficult to use initially, but felt it got easier over the course of the experiment ($P4, 17$).

7 APPLICATIONS

Complex 3D curves on arbitrary surfaces can be drawn in VR with a single stroke, using *mimicy* (Figure 16). Drawing such curves on 3D virtual objects is fundamental to many applications, including direct

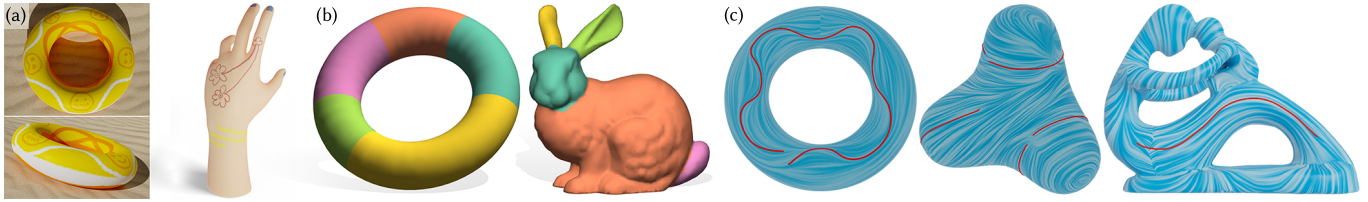


Fig. 18. Applications of *mimicry* projection. Texture painting (a), interactive segmentation by drawing curves onto meshes (b), and providing constraints (red curves) to guide the vector field generation of Fisher et al. [2007] (c).

painting of textures [Schmidt et al. 2006]; tangent vector field design [Fisher et al. 2007]; texture synthesis [Lefebvre and Hoppe 2006; Turk 2001]; interactive selection, annotation, and object segmentation [Chen et al. 2009]; and seams for shape parametrization [Lévy et al. 2002; Rabinovich et al. 2017; Sawhney and Crane 2017], registration [Gehre et al. 2018], and quad meshing [Tong et al. 2006]. We showcase the utility and quality of *mimicry* curves within example applications (also see supplemental video).

We also stress-test our technique by drawing curves on complex models (Figure 17a,b,e) and drawing a single long curve looping around the fertility model multiple times (Figure 17c). Finally, we show a failure case discussed in § 3.2—the *mimicry* projection fails catastrophically due to problems in the underlying π_{ACP} projection when the mesh is perturbed with excessive random noise (Figure 17d). Smaller local jumps can also occur when the model is both highly detailed and contains many sharp features (see inset in Figure 17e).

Texture Painting. Figures 1e, 18a show examples of textures painted in VR using *mimicry*. The long, smooth, wraparound curves on the torus, are especially hard to draw with 2D interfaces. Our implementation uses Discrete Exponential Maps (DEM) [Schmidt et al. 2006] to compute a dynamic local parametrization around each projected point q_i , to create brush strokes or geometric stamps on the object.

Mesh Segmentation. Figures 1e, 18b show interactive segmentation using *mimicry*. In our implementation, users draw an almost-closed curve $Q = \{q_0, \dots, q_{n-1}\}$ on the object using *mimicry*. We snap points q_i to their nearest mesh vertex, and use Dijkstra’s shortest path to connect consecutive vertices, and to close the cycle. While easy in VR via *mimicry*, drawing similar strokes in 2D for selection/segmentation would require multiple view changes.

Vector Field Design. Vector fields on meshes are commonly used for texture synthesis [Turk 2001], guiding fluid simulations [Stam 2003], and non-photorealistic rendering [Hertzmann and Zorin 2000]. We use *mimicry* curves as soft constraints to guide the vector field generation of Fisher et al. [2007]. Figure 18c shows example vector fields, visualized using Line Integral Convolutions [Cabral and Leedom 1993] in the texture domain.

8 CONCLUSION

We have presented a detailed investigation of the problem of real-time inked drawing on 3D virtual objects in immersive environments. We show the importance of stroke context when projecting

mid-air 3D strokes, and explore the design space of anchored projections. A 20-participant study showed *mimicry* to be preferred over the established *spraycan* projection for projecting 3D strokes onto objects in VR. Both *mimicry* projection and performing VR studies in the wild do have some limitations. Further, while user stroke processing for 2D interfaces is a mature field of research, mid-air stroke processing for AR/VR is relatively nascent, with many directions for future work. Our study contributes a high-quality VR data corpus comprising ≈ 2400 user strokes, projected curves, intended target curves, and corresponding system states, useful for future data-driven techniques for mid-air stroke processing.

“In the wild” VR Study Limitations. Ongoing pandemic restrictions presented both a challenge and an opportunity to remotely conduct a more natural study in the wild, with a variety of consumer VR hardware and setups. The enthusiasm of the VR community allowed us to readily recruit 20 diligent users, albeit with a bias towards young, adult males. While the variation in VR headsets seemed to be of little consequence, differences in controller grip and weight can certainly impact mid-air drawing posture and stroke behavior. Controller size is also significant: a larger Vive controller, for example, has a higher chance of occluding target objects and projected curves, as compared to a smaller Oculus Touch controller. We could have mitigated the impact of controller size by rendering a standard drawing tool, but we preferred to render the familiar, default controller that matched the physical device in participants’ hands. Further, no participant explicitly mentioned the controller getting in the way of their ability to draw.

Mimicry Limitations. Our lack of a concise mathematical definition of observed stroke mimicry, makes it harder to precisely communicate it to users. While a precise mathematical formulation may exist, conveying it to non-technical users can still be a challenging task. *Mimicry* ignores controller orientation, producing smoother strokes with less effort, but can give participants a reduced sense of sketch control ($P2,3,6$). We hypothesize that the reduced sense of control is in part due to the tendency for anchored smooth-closest-point to shorten the user stroke upon projection, sometimes creating a feeling of lag. *Spraycan* like techniques, in contrast, have a sense of amplified immediacy, and the explicit ability to make lagging curves catch-up by rotating a controller in place.

Future work. Our goal was to develop a general real-time inked projection with minimal stroke context via anchoring. Optimizing the method to account for the entire partially projected stroke may improve the projection quality. Relaxing the restriction of real-time

inking would allow techniques such as spline fitting and global optimization that can account for the entire user stroke and geometric features of the target object. Local parametrizations such as DEM (§ 7) can be used to incrementally grow or shrink the projected curve, so it does not lag the user stroke. Hybrid projections leveraging both proximity and raycasting are also subject to future work.

On the interactive side, we experimented with feedback to encourage users to draw closer to a 3D object. For example, we tried varying the appearance of the line connecting the controller to the projected point based on line length; or providing aural/haptic feedback if the controller got further than a certain distance from the object. While these techniques can help users in specific drawing or tracing tasks, we found them to be distracting and harmful to stroke quality for general stroke projection. Bimanual interaction, such as rotating the shape with one hand while drawing on it with the other (suggested by P3,19), can also be explored. To generalize our work to AR, the impact of rendering quality and perception of virtual models also needs to be studied in the future. Drawing on physical objects in AR is another related research direction.

Application-dependent optimizations to encourage closed strokes, snapping to geometric features, or alignment with existing user-drawn curves, can also be explored in the future. Further, our user study only focused on smooth curves. While we show author-drawn example of curves with sharp features (Figure 16), formally testing the *mimicry* technique for drawing such curves and potentially optimizing the projection to deal with sharp features is an important future direction. But perhaps the most exciting area of future work is data-driven techniques for inferring the intended projection, perhaps customized to the drawing style of individual users. Our study code and data has been made publicly available at github.com/rarora7777/curve-on-surface-drawing-vr to aid in such endeavours.

ACKNOWLEDGMENTS

We are thankful to Michelle Lei for developing the initial implementation of the context-free techniques, and to Jiannan Li and Debanjana Kundu for helping pilot our methods. We also thank various 3D model creators and repositories for the models we utilized: Stanford bunny and armadillo models courtesy of the Stanford 3D Scanning Repository, trebol model provided by Shao et al. [2012], fertility model courtesy the Aim@Shape repository, hand model provided by Jeffo89 on turbosquid.com, horse model courtesy Cyberware, Spiderman bust base model by David Ruiz Olivares (CC BY 4.0), beast model courtesy Autodesk, fandisk model provided by Pratt & Whitney/Hughes Hoppe, La Madeleine model by LeFab-Shop on thingiverse.com (CC BY-SA 3.0), and cup model (Figure 2) provided by Daniel Noree on thingiverse.com (CC BY 4.0).

This work has been funded by NSERC Discovery Grant 480538, and by software and research donations from Adobe.

REFERENCES

- Adobe. 2020. Substance Painter. <https://www.substance3d.com/substance-painter/>
- Adobe. 2021. Medium by Adobe. <https://www.adobe.com/products/medium.html>
- Alexis Andre and Suguru Saito. 2011. Single-View Sketch Based Modeling. In *Proceedings of the Eighth Eurographics Symposium on Sketch-Based Interfaces and Modeling* (Vancouver, British Columbia, Canada) (SBIM '11). Association for Computing Machinery, New York, NY, USA, 133–140. <https://doi.org/10.1145/2021164.2021189>
- Rahul Arora, Rubaiat Habib Kazi, Fraser Anderson, Tovi Grossman, Karan Singh, and George Fitzmaurice. 2017. Experimental Evaluation of Sketching on Surfaces in VR. In *Proceedings of the 2017 CHI Conference on Human Factors in Computing Systems* (Denver, Colorado, USA) (CHI '17). Association for Computing Machinery, New York, NY, USA, 5643–5654. <https://doi.org/10.1145/3025453.3025474>
- Rahul Arora, Rubaiat Habib Kazi, Tovi Grossman, George Fitzmaurice, and Karan Singh. 2018. SymbiosisSketch: Combining 2D & 3D Sketching for Designing Detailed 3D Objects in Situ. In *Proceedings of the 2018 CHI Conference on Human Factors in Computing Systems* (Montreal, Quebec, Canada) (CHI '18). ACM, New York, NY, USA, 15 pages. <https://doi.org/10.1145/3173574.3173759>
- Seok-Hyung Bae, Ravin Balakrishnan, and Karan Singh. 2008. ILoveSketch: as-natural-as-possible sketching system for creating 3D curve models. In *Proceedings of the 21st annual ACM symposium on User interface software and technology* (Monterey, CA, USA) (UIST '08). ACM, New York, NY, USA, 151–160. <https://doi.org/10.1145/1449715.1449740>
- Gavin Barill, Neil G. Dickson, Ryan Schmidt, David I. W. Levin, and Alec Jacobson. 2018. Fast Winding Numbers for Soups and Clouds. *ACM Trans. Graph.* 37, 4, Article 43 (July 2018), 12 pages. <https://doi.org/10.1145/3197517.3201337>
- Brian Cabral and Leith Casey Leedom. 1993. Imaging Vector Fields Using Line Integral Convolution. In *Proceedings of the 20th Annual Conference on Computer Graphics and Interactive Techniques* (Anaheim, CA) (SIGGRAPH '93). Association for Computing Machinery, New York, NY, USA, 263–270. <https://doi.org/10.1145/166117.166151>
- Tao Chen, Zhe Zhu, Ariel Shamir, Shi-Min Hu, and Daniel Cohen-Or. 2013. 3-Sweep: Extracting Editable Objects from a Single Photo. *ACM Trans. Graph.* 32, 6, Article 195 (Nov. 2013), 10 pages. <https://doi.org/10.1145/2508363.2508378>
- Xiaobai Chen, Aleksey Golovinskiy, and Thomas Funkhouser. 2009. A Benchmark for 3D Mesh Segmentation. *ACM Trans. Graph.* 28, 3, Article 73 (July 2009), 12 pages. <https://doi.org/10.1145/1531326.1531379>
- Patrick Coleman and Karan Singh. 2006. Cords: Geometric Curve Primitives for Modeling Contact. *IEEE Computer Graphics and Applications* 26, 3 (2006), 72–79.
- Michael AA Cox and Trevor F Cox. 2008. Multidimensional scaling. In *Handbook of data visualization*. Springer, New York, NY, USA, 315–347.
- Chris De Paoli and Karan Singh. 2015. SecondSkin: Sketch-Based Construction of Layered 3D Models. *ACM Trans. Graph.* 34, 4, Article 126 (July 2015), 10 pages. <https://doi.org/10.1145/2766948>
- Michael F Deering. 1995. HoloSketch: a virtual reality sketching/animation tool. *ACM Transactions on Computer-Human Interaction (TOCHI)* 2, 3 (1995), 220–238.
- Lubin Fan, Ruimin Wang, Linlin Xu, Jiansong Deng, and Ligang Liu. 2013. Modeling by Drawing with Shadow Guidance. *Computer Graphics Forum* 32, 7 (2013), 157–166. <https://doi.org/10.1111/cgf.12223>
- Zhe Fan, Ma Chi, Arie Kaufman, and Manuel M. Oliveira. 2004. A Sketch-Based Interface for Collaborative Design. In *Sketch Based Interfaces and Modeling*. The Eurographics Association, Geneva, Switzerland, 143–150. <https://doi.org/10.2312/SBM/SBM04/143-150>
- Matthew Fisher, Peter Schröder, Mathieu Desbrun, and Hugues Hoppe. 2007. Design of Tangent Vector Fields. *ACM Trans. Graph.* 26, 3 (July 2007), 56–es. <https://doi.org/10.1145/1276377.1276447>
- Hongbo Fu, Yichen Wei, Chiew-Lan Tai, and Long Quan. 2007. Sketching Hairstyles. In *Proceedings of the 4th Eurographics Workshop on Sketch-Based Interfaces and Modeling* (Riverside, California) (SBIM '07). Association for Computing Machinery, New York, NY, USA, 31–36. <https://doi.org/10.1145/1384429.1384439>
- Ran Gal, Olga Sorkine, Niloy J. Mitra, and Daniel Cohen-Or. 2009. iWIRES: An Analyze-and-Edit Approach to Shape Manipulation. *ACM Transactions on Graphics (Siggraph)* 28, 3 (2009), #33, 1–10.
- Anne Gehre, Michael Bronstein, Leif Kobbelt, and Justin Solomon. 2018. Interactive Curve Constrained Functional Maps. *Computer Graphics Forum* 37, 5 (2018), 1–12. <https://doi.org/10.1111/cgf.13486>
- Bruce Gooch and Amy Gooch. 2001. *Non-Photorealistic Rendering*. A. K. Peters, USA.
- Google. 2020. Tilt Brush by Google. <https://www.tiltbrush.com/>
- Gravity Sketch. 2020. Gravity Sketch. <https://www.gravitysketch.com/>
- Tovi Grossman, Ravin Balakrishnan, Gordon Kurtenbach, George Fitzmaurice, Azam Khan, and Bill Buxton. 2002. Creating Principal 3D Curves with Digital Tape Drawing. In *Proceedings of the SIGCHI Conference on Human Factors in Computing Systems* (Minneapolis, Minnesota, USA) (CHI '02). ACM, New York, NY, USA, 121–128. <https://doi.org/10.1145/503376.503398>
- Frank Heckel, Jan H. Moltz, Christian Tietjen, and Horst K. Hahn. 2013. Sketch-Based Editing Tools for Tumour Segmentation in 3D Medical Images. *Computer Graphics Forum* 32, 8 (2013), 144–157. <https://doi.org/10.1111/cgf.12193>
- Aaron Hertzmann and Denis Zorin. 2000. Illustrating Smooth Surfaces. In *Proceedings of the 27th Annual Conference on Computer Graphics and Interactive Techniques (SIGGRAPH '00)*. ACM Press/Addison-Wesley Publishing Co., USA, 517–526. <https://doi.org/10.1145/344779.345074>
- Yixin Hu, Qingnan Zhou, Xifeng Gao, Alec Jacobson, Denis Zorin, and Daniele Panozzo. 2018. Tetrahedral Meshing in the Wild. *ACM Trans. Graph.* 37, 4, Article 60 (July 2018), 14 pages. <https://doi.org/10.1145/3197517.3201353>

- Takeo Igarashi, Satoshi Matsuoka, and Hidehiko Tanaka. 1999. Teddy: A Sketching Interface for 3D Freeform Design. In *Proceedings of the 26th Annual Conference on Computer Graphics and Interactive Techniques (SIGGRAPH '99)*. ACM Press/Addison-Wesley Publishing Co., USA, 409–416. <https://doi.org/10.1145/311535.311602>
- Bret Jackson and Daniel F Keefe. 2016. Lift-off: Using Reference Imagery and Freehand Sketching to Create 3D Models in VR. *IEEE transactions on visualization and computer graphics* 22, 4 (2016), 1442–1451.
- Alec Jacobson, Daniele Panozzo, et al. 2018. libigl: A simple C++ geometry processing library. <https://libigl.github.io/>.
- Zhongshi Jiang, Teseo Schneider, Denis Zorin, and Daniele Panozzo. 2020. Bijective Projection in a Shell. *ACM Trans. Graph.* 39, 6, Article 247 (Nov. 2020), 18 pages. <https://doi.org/10.1145/3414685.3417769>
- Yao Jin, Dan Song, Tongtong Wang, Jin Huang, Ying Song, and Lili He. 2019. A shell space constrained approach for curve design on surface meshes. *Computer-Aided Design* 113 (2019), 24–34. <https://doi.org/10.1016/j.cad.2019.03.001>
- Thomas Jung, Mark D. Gross, and Ellen Yi-Luen Do. 2002. Annotating and Sketching on 3D Web Models. In *Proceedings of the 7th International Conference on Intelligent User Interfaces* (San Francisco, California, USA) (IUI '02). Association for Computing Machinery, New York, NY, USA, 95–102. <https://doi.org/10.1145/502716.502733>
- Robert D. Kalnins, Lee Markosian, Barbara J. Meier, Michael A. Kowalski, Joseph C. Lee, Philip L. Davidson, Matthew Webb, John F. Hughes, and Adam Finkelstein. 2002. WYSIWYG NPR: Drawing Strokes Directly on 3D Models. *ACM Trans. Graph.* 21, 3 (July 2002), 755–762. <https://doi.org/10.1145/566654.566648>
- Sho Kamuro, Kouta Minamizawa, and Susumu Tachi. 2011. 3D Haptic Modeling System using Ungrounded Pen-shaped Kinesthetic Display. In *2011 IEEE Virtual Reality Conference*. IEEE, New York, NY, USA, 217–218.
- Levent Burak Kara and Kenji Shimada. 2007. Sketch-Based 3D-Shape Creation for Industrial Styling Design. *IEEE Comput. Graph. Appl.* 27, 1 (Jan. 2007), 60–71. <https://doi.org/10.1109/MCG.2007.18>
- Daniel Keefe, Robert Zeleznik, and David Laidlaw. 2007. Drawing on Air: Input Techniques for Controlled 3D Line Illustration. *IEEE Transactions on Visualization and Computer Graphics* 13, 5 (2007), 1067–1081.
- Daniel F. Keefe, Daniel Acevedo Feliz, Tomer Moscovich, David H. Laidlaw, and Joseph J. LaViola. 2001. CavePainting: A Fully Immersive 3D Artistic Medium and Interactive Experience. In *Proceedings of the 2001 Symposium on Interactive 3D Graphics (I3D '01)*. Association for Computing Machinery, New York, NY, USA, 85–93. <https://doi.org/10.1145/364338.364370>
- Venkat Krishnamurthy and Marc Levoy. 1996. Fitting Smooth Surfaces to Dense Polygon Meshes. In *Proceedings of the 23rd Annual Conference on Computer Graphics and Interactive Techniques (SIGGRAPH '96)*. Association for Computing Machinery, New York, NY, USA, 313–324. <https://doi.org/10.1145/237170.237270>
- Vojtěch Krs, Ersin Yumer, Nathan Carr, Bedrich Benes, and Radomír Měch. 2017. Skippy: Single View 3D Curve Interactive Modeling. *ACM Trans. Graph.* 36, 4, Article 128 (July 2017), 12 pages. <https://doi.org/10.1145/3072959.3073603>
- Kin Chung Kwan and Hongbo Fu. 2019. Mobi3DSketch: 3D Sketching in Mobile AR. In *Proceedings of the 2019 CHI Conference on Human Factors in Computing Systems* (Glasgow, Scotland, UK) (CHI '19). Association for Computing Machinery, New York, NY, USA, 1–11. <https://doi.org/10.1145/3290605.3300406>
- Sylvain Lefebvre and Hugues Hoppe. 2006. Appearance-Space Texture Synthesis. *ACM Trans. Graph.* 25, 3 (July 2006), 541–548. <https://doi.org/10.1145/1141911.1141921>
- Bruno Lévy, Sylvain Petitjean, Nicolas Ray, and Jérôme Maillot. 2002. Least Squares Conformal Maps for Automatic Texture Atlas Generation. *ACM Trans. Graph.* 21, 3 (July 2002), 362–371. <https://doi.org/10.1145/566654.566590>
- Mayra D. Barrera Machuca, Paul Asente, Wolfgang Stuerzlinger, Jingwan Lu, and Byungmoon Kim. 2018. Multiplanes: Assisted Freehand VR Sketching. In *Proceedings of the Symposium on Spatial User Interaction* (Berlin, Germany) (SUI '18). Association for Computing Machinery, New York, NY, USA, 36–47. <https://doi.org/10.1145/3267782.3267786>
- Mayra Donaji Barrera Machuca, Wolfgang Stuerzlinger, and Paul Asente. 2019. The Effect of Spatial Ability on Immersive 3D Drawing. In *Proceedings of the ACM Conference on Creativity & Cognition (C&C'19)*. ACM, New York, NY, USA, 173–186.
- James McCrae and Karan Singh. 2008. Sketching Piecewise Clothoid Curves. In *Proceedings of the Fifth Eurographics Conference on Sketch-Based Interfaces and Modeling* (Annecy, France) (SBM'08). Eurographics Association, Goslar, DEU, 1–8.
- James McCrae, Karan Singh, and Niloy J. Mitra. 2011. Slices: A Shape-Proxy Based on Planar Sections. *ACM Trans. Graph.* 30, 6 (Dec. 2011), 1–12. <https://doi.org/10.1145/2070781.2024202>
- James McCrae, Nobuyuki Umetani, and Karan Singh. 2014. FlatFitFab: Interactive Modeling with Planar Sections. In *Proceedings of the 27th Annual ACM Symposium on User Interface Software and Technology* (Honolulu, Hawaii, USA) (UIST '14). Association for Computing Machinery, New York, NY, USA, 13–22. <https://doi.org/10.1145/2642918.2647388>
- Min Meng, Lubin Fan, and Ligang Liu. 2011. iCutter: A Direct Cut-out Tool for 3D Shapes. *Computer Animation and Virtual Worlds* 22, 4 (2011), 335–342. <https://doi.org/10.1002/cav.422>
- Andrew Nealen, Takeo Igarashi, Olga Sorkine, and Marc Alexa. 2007. FiberMesh: Designing Freeform Surfaces with 3D Curves. *ACM Trans. Graph.* 26, 3 (July 2007), 41–es. <https://doi.org/10.1145/1276377.1276429>
- Oculus. 2020. Quill. <https://www.oculus.com/experiences/rift/1118609381580656/>
- Luke Olsen, Faramarz F. Samavati, Mario Costa Sousa, and Joaquim A. Jorge. 2009. Sketch-based Modeling: A survey. *Computers and Graphics* 33, 1 (2009), 85–103. <https://doi.org/10.1016/j.cag.2008.09.013>
- Michael Ortega and Thomas Vincent. 2014. Direct Drawing on 3D Shapes with Automated Camera Control. In *Proceedings of the SIGCHI Conference on Human Factors in Computing Systems* (Toronto, Canada) (CHI '14). Association for Computing Machinery, New York, NY, USA, 2047–2050. <https://doi.org/10.1145/2556288.2557242>
- Patrick Paczkowski, Min H. Kim, Yann Morvan, Julie Dorsey, Holly Rushmeier, and Carol O'Sullivan. 2011. Insitu: Sketching Architectural Designs in Context. *ACM Trans. Graph.* 30, 6 (Dec. 2011), 1–10. <https://doi.org/10.1145/2070781.2024216>
- Daniele Panozzo, Ilya Baran, Olga Diamanti, and Olga Sorkine-Hornung. 2013. Weighted Averages on Surfaces. *ACM Trans. Graph.* 32, 4, Article 60 (July 2013), 12 pages. <https://doi.org/10.1145/2461912.2461935>
- Konrad Polthier and Markus Schmies. 2006. Straightest Geodesics on Polyhedral Surfaces. In *ACM SIGGRAPH 2006 Courses* (Boston, Massachusetts) (SIGGRAPH '06). Association for Computing Machinery, New York, NY, USA, 30–38. <https://doi.org/10.1145/1185657.1185664>
- Michael Rabinovich, Roi Poranne, Daniele Panozzo, and Olga Sorkine-Hornung. 2017. Scalable Locally Injective Mappings. *ACM Trans. Graph.* 36, 2, Article 16 (April 2017), 16 pages. <https://doi.org/10.1145/2983621>
- Rohan Sawhney and Keenan Crane. 2017. Boundary First Flattening. *ACM Trans. Graph.* 37, 1, Article 5 (Dec. 2017), 14 pages. <https://doi.org/10.1145/3132705>
- Steven Schkolne, Michael Pruett, and Peter Schröder. 2001. Surface Drawing: Creating Organic 3D Shapes with the Hand and Tangible Tools. In *Proceedings of the SIGCHI conference on Human factors in computing systems*. ACM, New York, NY, USA, 261–268.
- Johannes Schmid, Martin Sebastian Senn, Markus Gross, and Robert W. Sumner. 2011. OverCoat: An Implicit Canvas for 3D Painting. *ACM Trans. Graph.* 30, 4, Article 28 (July 2011), 10 pages. <https://doi.org/10.1145/2010324.1964923>
- Ryan Schmidt. 2017. geometry3sharp: Open-Source (Boost-license) C# Library for Geometric Computing. <https://github.com/gradientspace/geometry3Sharp>.
- Ryan Schmidt, Cindy Grimm, and Brian Wyvill. 2006. Interactive Decal Compositing with Discrete Exponential Maps. *ACM Trans. Graph.* 25, 3 (July 2006), 605–613. <https://doi.org/10.1145/1141911.1141930>
- Ryan Schmidt, Azam Khan, Karan Singh, and Gord Kurtenbach. 2009. Analytic Drawing of 3D Scaffolds. In *ACM SIGGRAPH Asia 2009 Papers* (Yokohama, Japan) (SIGGRAPH Asia '09). Association for Computing Machinery, New York, NY, USA, Article 149, 10 pages. <https://doi.org/10.1145/1661412.1618495>
- Ryan Schmidt and Karan Singh. 2010. Meshmixer: An Interface for Rapid Mesh Composition. In *ACM SIGGRAPH 2010 Talks* (Los Angeles, California) (SIGGRAPH '10). ACM, New York, NY, USA, Article 6, 1 pages. <https://doi.org/10.1145/1837026.1837034>
- Cloud Shao, Adrien Bousseau, Alla Sheffer, and Karan Singh. 2012. CrossShade: Shading Concept Sketches Using Cross-section Curves. *ACM Trans. Graph.* 31, 4, Article 45 (July 2012), 11 pages. <https://doi.org/10.1145/2185520.2185541>
- Hang Si. 2015. TetGen, a Delaunay-Based Quality Tetrahedral Mesh Generator. *ACM Trans. Math. Softw.* 41, 2, Article 11 (Feb. 2015), 36 pages. <https://doi.org/10.1145/2629697>
- Karan Singh and Eugene Fiume. 1998. Wires: A Geometric Deformation Technique. In *Proceedings of the 25th Annual Conference on Computer Graphics and Interactive Techniques, SIGGRAPH 1998, Orlando, FL, USA, July 19-24, 1998*, Steve Cunningham, Walt Bransford, and Michael F. Cohen (Eds.). ACM, New York, NY, USA, 405–414. <https://doi.org/10.1145/280814.280946>
- Olga Sorkine and Daniel Cohen-Or. 2004. Least-squares Meshes. In *Proceedings of Shape Modeling International* (Genova, Italy). IEEE Computer Society Press, Piscataway, NJ, USA, 191–199.
- Jos Stam. 2003. Flows on Surfaces of Arbitrary Topology. In *ACM SIGGRAPH 2003 Papers* (San Diego, California) (SIGGRAPH '03). Association for Computing Machinery, New York, NY, USA, 724–731. <https://doi.org/10.1145/1201775.882338>
- Lucian Stanculescu, Raphaëlle Chaine, Marie-Paule Ciani, and Karan Singh. 2013. Sculpting Multi-dimensional Nested Structures. *Comput. Graph.-UK* 37, 6 (Oct. 2013), 753–763. Special issue: Shape Modeling International (SMI) Conference 2013.
- Vitaly Surazhsky, Tatiana Surazhsky, Danil Kirsanov, Steven J. Gortler, and Hugues Hoppe. 2005. Fast Exact and Approximate Geodesics on Meshes. *ACM Trans. Graph.* 24, 3 (July 2005), 553–560. <https://doi.org/10.1145/1073204.1073228>
- Kenshi Takayama, Daniele Panozzo, Alexander Sorkine-Hornung, and Olga Sorkine-Hornung. 2013. Sketch-based Generation and Editing of Quad Meshes. *ACM Trans. Graph.* 32, 4, Article 97 (July 2013), 8 pages. <https://doi.org/10.1145/2461912.2461955>
- Yannick Thiel, Karan Singh, and Ravin Balakrishnan. 2011. Elasticurves: Exploiting Stroke Dynamics and Inertia for the Real-Time Neatening of Sketched 2D Curves. In *Proceedings of the 24th Annual ACM Symposium on User Interface Software and Technology* (Santa Barbara, California, USA) (UIST '11). Association for Computing Machinery, New York, NY, USA, 383–392. <https://doi.org/10.1145/2047196.2047246>

- Yiyong Tong, Pierre Alliez, David Cohen-Steiner, and Mathieu Desbrun. 2006. Designing Quadragulations with Discrete Harmonic Forms. In *Proceedings of the Fourth Eurographics Symposium on Geometry Processing* (Cagliari, Sardinia, Italy) (SGP '06). Eurographics Association, Goslar, DEU, 201–210.
- Greg Turk. 2001. Texture Synthesis on Surfaces. In *Proceedings of the 28th Annual Conference on Computer Graphics and Interactive Techniques (SIGGRAPH '01)*. Association for Computing Machinery, New York, NY, USA, 347–354. <https://doi.org/10.1145/383259.383297>
- Emmanuel Turquin, Jamie Wither, Laurence Boissieux, Marie-Paule Cani, and John F. Hughes. 2007. A Sketch-Based Interface for Clothing Virtual Characters. *IEEE Comput. Graph. Appl.* 27, 1 (Jan. 2007), 72–81. <https://doi.org/10.1109/MCG.2007.1>
- Gerold Wesche and Hans-Peter Seidel. 2001. FreeDrawer: A Free-form Sketching System on the Responsive Workbench. In *Proceedings of the ACM symposium on Virtual reality software and technology*. ACM, New York, NY, USA, 167–174.
- Eva Wiese, Johann Habakuk Israel, Achim Meyer, and Sara Bongartz. 2010. Investigating the Learnability of Immersive Free-Hand Sketching. In *Proceedings of the Seventh Sketch-Based Interfaces and Modeling Symposium (Annecy, France) (SBIM '10)*. Eurographics Association, Goslar, DEU, 135–142.
- Jun Xing, Koki Nagano, Weikai Chen, Haotian Xu, Li-yi Wei, Yajie Zhao, Jingwan Lu, Byungmoon Kim, and Hao Li. 2019. HairBrush for Immersive Data-Driven Hair Modeling. In *Proceedings of the 32nd Annual ACM Symposium on User Interface Software and Technology* (New Orleans, LA, USA) (UIST '19). Association for Computing Machinery, New York, NY, USA, 263–279. <https://doi.org/10.1145/3332165.3347876>
- Baoxuan Xu, William Chang, Alla Sheffer, Adrien Bousseau, James McCrae, and Karan Singh. 2014. True2Form: 3D Curve Networks from 2D Sketches via Selective Regularization. *ACM Trans. Graph.* 33, 4, Article 131 (July 2014), 13 pages. <https://doi.org/10.1145/2601097.2601128>

A CONTEXT-FREE PILOT OBSERVATIONS

In this appendix, we provide additional informal observations from our pilot tests with context-free techniques (Section 3.1), as well as additional details on the limitations of such techniques.

A.1 Qualitative observations

- *Head-centric* and *occlude* projections become unpredictable if the user is inadvertently changing their viewpoint while drawing. These projections are also only effective when drawing frontally on an object, like with a 2D interface. Neither as a result exploits the potential gains of mid-air drawing in AR/VR.
- *Spraycan* projection was clearly the most effective context-free technique. We noted however, that consciously reorienting the controller while drawing on or around complex objects was both cognitively and physically tiring.
- *Snap* projection was quite sensitive to changes in the distance of the stroke from the object surface, and in general produced the most undulating projections due to closest-point singularities.
- All projections converge to the mid-air user stroke when it precisely conforms to the surface of the 3D object. But as the distance between the object and points on the mid-air stroke increases, their behavior diverges quickly.
- While users did draw in the vicinity and mostly above the object surface, they rarely drew precisely on the object. The average distance of stroke points from the target object was observed to be 4.8 cm in a subsequent user study (§ 5).

A.2 Details on the Limitations of Context-Free Methods

The inability of context-free approaches to capture a notion of stroke mimicry—due to a lack of curve history or context—materializes as problems in different forms.

A.2.1 Projection Discontinuities. Proximal projection (including *smooth-closest-point*) can be highly discontinuous with increasing

distance from the 3D object, particularly in concave regions (Figure 5a). Mid-air drawing along valleys without staying in precise contact with virtual object is thus extremely difficult. Raycast projections can similarly suffer large discontinuous jumps across occluded regions (in the ray direction) of the object (Figure 5d).

While this problem theoretically exists in 2D interfaces as well, it is less observed in practice for two reasons: 2D drawing on a constraining physical surface is significantly more precise than mid-air drawing in AR/VR [Arora et al. 2017]; and artists minimize such discontinuities by carefully choosing appropriate views (raycast directions) before drawing each curve. Automatic direction control of view or controller, while effective in 2D [Ortega and Vincent 2014]), is detrimental to a sense of agency and presence in AR/VR.

A.2.2 Undesirable Snapping. Proximity-based methods also tend to get stuck on sharp (or high curvature) convex features of the object (Figure 5b). While this can be useful to trace along a ridge feature, it is particularly problematic for general curve-on-surface drawing.

A.2.3 Projection depth disparity. The relative orientation between the 3D object surface and raycast direction can cause large depth disparities between parts of user strokes and curves projected by raycasting (Figure 5c). Such irregular bunching or spreading of points on the projected curve also goes against our observation of stroke mimicry. Users can arguably reduce this disparity by continually orienting the view/controller to keep the projection ray well aligned with object surface normal. Such re-orientation however can be tiring, ergonomically awkward, and deviates from 2D experience, where pen/brush tilt only impacts curve aesthetic, and not shape.

B SAMPLING TARGET CURVES FOR THE USER STUDY

We wanted to design target curves that could be executed using a single smooth motion. Since users typically draw sharp corners using multiple strokes [Bae et al. 2008], we constrain our target curves to be smooth, created using cardinal cubic B-splines on the meshes, computed using Panozzo et al. [2013]. We also control the length and curvature complexity of the curves, as pilot testing showed that very simple and short curves can be reasonably executed by almost any projection technique. Curve length and complexity is modeled by placing spline control points at mesh vertices, and specifying the desired geodesic distance and Gauß map distance between consecutive control points on the curve.

We represent a target curve using four parameters $\langle n, i_0, k_G, k_N \rangle$, where n is the number of spline control points, i_0 the vertex index of the first control point, and k_G, k_N constants that control the geodesic and normal map distance between consecutive control points. We define the desired geodesic distance between consecutive control points as, $D_G = k_G \times \|\text{BBox}(\mathcal{M})\|$, where $\|\text{BBox}(\mathcal{M})\|$ is the length of the bounding box diagonal of \mathcal{M} . The desired Gauß map distance (angle between the unit vertex normals) between consecutive control points is simply k_N .

A target curve C_0, \dots, C_{n-1} starting at vertex v_{i_0} of the mesh is generated incrementally for $i > 0$ as:

$$C_i = \arg \min_{v \in V'} (d_G(C_{i-1}, v) - D_G)^2 + (d_N(C_{i-1}, v) - k_N)^2, \quad (11)$$

where d_G and d_N compute the geodesic and normal distance between two points on \mathcal{M} , and $V' \subset V$ contains only those vertices of \mathcal{M} whose geodesic distance from C_0, \dots, C_{i-1} is at least $D_G/2$. The restricted subset of vertices conveniently helps prevent (but doesn't fully avoid) self-intersecting or nearly self-intersecting curves. Curves with complex self-intersections are less important practically, and can be particularly confusing for the curve re-creation task. All our target curve samples were generated using $k_G \in [0.05, 0.25]$, $k_N \in [\pi/6, 5\pi/12]$, $n = 6$, and a randomly chosen i_0 . The curves were manually inspected for self-intersections, and infringing curves rejected.

We then defined keypoints on the target curves as follows: curve endpoints were chosen as keypoints; followed by greedily picking extrema of geodesic curvature, while ensuring that the arclength distance between any two consecutive keypoints was at least 3cm; and concluding the procedure when the maximum arclength distance between any consecutive keypoints was below 15cm. Our target curves had between 4–9 keypoints (including endpoints).

C ADDITIONAL QUANTITATIVE ANALYSES

C.1 Quantifying Users' Tendency to Mimic

The study also provided an opportunity to test if the users actually tended to mimic their intended curve \mathcal{X} in the mid-air stroke \mathcal{P} . To quantify the ‘‘mimcriness’’ of a stroke, we subsample \mathcal{P} and \mathcal{X}

into m points as in § 6.2.1, use the correspondence as in Eq. 7 and look at the variation in the distance (distance between the closest pair of corresponding points subtracted from that of the farthest pair) as a percentage of the target length $L_{\mathcal{X}}$. We call this measure the *mimicry violation* of a stroke. Intuitively, the lower the *mimicry violation*, the closer the stroke \mathcal{P} is to being a perfect mimicry of \mathcal{X} , going to zero if it is a precise translation of \mathcal{X} . Notably, users depicted very similar trends to mimic for both the techniques—with 86% (*mimicry*), 80% (*spraycan*) strokes exhibiting *mimicry violation* below 25% of $L_{\mathcal{X}}$, and 71%, 66% below 20% of $L_{\mathcal{X}}$ —suggesting that mimicry is indeed a natural tendency.

C.2 Consistency across Repeated Strokes

Recall that users repeated 2 of the 10 strokes per shape for both the techniques. To analyze consistency across the repeated strokes, we compared the values of the stroke accuracy measure D_{eq} and the aesthetic measure F_g between the original stroke and the corresponding repeated stroke. Specifically, we measured the relative change $|f(i) - f(i')|/f(i)$, where (i, i') is a pair of original and repeated strokes, and $f(\cdot)$ is either D_{eq} or F_g . Users were fairly consistent across both the techniques, with the average consistency for D_{eq} being 35.4% for *mimicry* and 36.8% for *spraycan*, while for F_g , it was 36.5% and 34.1%, respectively. Note that the averages were computed after removing extreme outliers outside the 5σ threshold.